

X-ray resonant magnetic scattering from structurally and magnetically rough interfaces in multilayered systems

I. Specular reflectivity

D. R. Lee,* D. Haskel, Y. Choi,[†] J. C. Lang, S. A. Stepanov, and G. Srajer
Advanced Photon Source, Argonne National Laboratory, Argonne, Illinois 60439

S. K. Sinha

Department of Physics, University of California,

San Diego, La Jolla, CA 92093, and

Los Alamos National Laboratory, Los Alamos, NM 87545

(Dated: November 4, 2018)

Abstract

The theoretical formulation of x-ray resonant magnetic scattering from rough surfaces and interfaces is given for specular reflectivity. A general expression is derived for both structurally and magnetically rough interfaces in the distorted-wave Born approximation (DWBA) as the framework of the theory. For this purpose, we have defined a “structural” and a “magnetic” interface to represent the actual interfaces. A generalization of the well-known Nevot-Croce formula for specular reflectivity is obtained for the case of a single rough magnetic interface using the self-consistent method. Finally, the results are generalized to the case of multiple interfaces, as in the case of thin films or multilayers. Theoretical calculations for each of the cases are illustrated with numerical examples and compared with experimental results of magnetic reflectivity from a Gd/Fe multilayer.

I. INTRODUCTION

X-ray reflectivity and offspecular diffuse scattering methods have been widely applied over the last decade to characterize the morphology of rough surfaces and interfaces, particularly with the availability of sources of ever-increasing brilliance for x-ray radiation. Similar techniques using neutron beams have also become widespread, particularly for the study of magnetic multilayers. In the case of x-rays, however, element-specific information regarding the magnetic structure can be readily obtained by tuning the photon energy to that of an L-edge (in the case of transition or rare-earth metals)^{1,2} or of an M-edge (in the case of actinides).^{3,4} The resonant enhancement of the scattering by magnetic atoms at such energies can result in a large enough signal to be comparable to the dominant charge scattering. Resonant x-ray scattering at the K-edges of transition metals⁵ has also been used to obtain information about the magnetic structure, although the enhancement is not as large. Resonant magnetic scattering corresponds to the real part of the scattering amplitude, while the (absorptive) imaginary part gives rise to x-ray magnetic circular dichroism (XMCD), which has been used to obtain the values of spin and orbital moments in ferromagnetic materials. Detailed descriptions of the formalism for the interaction of x-rays with magnetically polarized atoms have been given in the literature,⁶⁻¹⁰ from which a complete description of magneto-optic phenomena in the x-ray region can be obtained and applied.

Several resonant x-ray specular reflectivity experiments have been performed to obtain the magnetization within the layers of magnetic multilayers.^{2,11-14} The analysis of these results has generally used recursive matrix techniques developed for magneto-optics in the case of resonant x-ray reflectivity.¹⁵ In general, roughness at the interfaces has been ignored or taken into account in an ad-hoc manner. In principle, representing roughness in terms of a graded magnetization at the interface and using slicing methods could enable one to calculate the effect of magnetic roughness on specular reflectivity at the expense of considerable computational effort. Röhlsberger has developed a matrix formalism (originally developed for nuclear resonant x-ray reflectivity) from which specular reflectivity incorporating roughness can be calculated.¹⁶ It was not considered in his paper, however, that the magnetic interfaces can have different roughnesses from the structural (chemical) ones. In this paper, we define separately a structural and a magnetic interface to represent the actual interfaces and present analytical formulae taking into account both interface roughnesses,

which provide much faster computational method than the slicing methods and show good agreement with established formulae for chemical interface roughness.

Methods were developed earlier to calculate analytically the specular component of the charge scattering of x-rays by rough surfaces and interfaces using the Born approximation (BA) and the distorted-wave Born approximation (DWBA).^{17,18} The BA results were extended to magnetic interfaces in an earlier publication¹⁹ and have already been applied to interpreting x-ray resonant magnetic specular reflectivity measurements from magnetic multilayers.¹⁴ However, the BA or the kinematical approximation breaks down in the vicinity of the critical angle and below, since it neglects the x-ray refraction. On the other hand, the DWBA takes account of dynamical effects, such as multiple scattering and the x-ray refraction, which become significant for smaller angles close to the critical angle and even for greater angles at the resonant energies or with soft x-rays. We present here the generalization of the DWBA to the case of resonant magnetic x-ray reflectivity from rough magnetic surfaces or interfaces. The principal complication is, however, that we now have to deal with a tensor (rather than scalar) scattering length, or equivalently an anisotropic refractive index for x-rays.¹⁵ This leads in general to two transmitted and two reflected waves at each interface for arbitrary polarization, which complicates the DWBA formalism.

The plan of this paper is as follows. In Sec. II, we discuss a simple conceptual model for a magnetic interface and its relationship to the chemical (i.e., structural) interface and define the appropriate magnetic roughness parameters. In Sec. III, we discuss the (known) scattering amplitudes for resonant x-ray scattering and their relationship to the dielectric susceptibility to be used in the DWBA. In Sec. IV, we present the derivation of the scattering in the DWBA for a single interface with both structural and magnetic roughnesses. In Secs. V and VI, we derive the formulae for specular reflectivity from a magnetic interface using the self-consistent method in the framework of the DWBA and discuss numerical results. Finally, in Secs. VII-IX, we discuss the extension of the formalism to the case of the specular reflectivity from magnetic multilayers and present some numerical results with experimental data from a Gd/Fe multilayer. In the following paper,²⁰ we derive the formulae for the diffuse (off-specular) scattering from magnetic interfaces in both the BA and the DWBA.

II. MODEL FOR MAGNETIC INTERFACE

Consider an interface between a ferromagnetic medium and a nonmagnetic medium (which could also be free space). Due to the roughness of this interface, the magnetic moments near the interface will find themselves in anisotropy and exchange fields, which fluctuate spatially (see Fig. 1).

This will produce disorder relative to the preferred ferromagnetic alignment within the magnetic medium. A similar situation can arise at an interface between a ferromagnetic medium (FM) and an antiferromagnetic medium (AFM), where there is a strong antiferromagnetic coupling between spins in the FM and the AFM. Random steps will then produce frustration in the vicinity of the interface, resulting in random disordering of the magnetic moments near the interface. Clearly in general correlation will exist between the height fluctuations of the chemical interface and the fluctuations of the spins, but a quantitative formalism to account for this in detail has not yet been developed. We make here the simplifying assumption that the ferromagnetic moments near the interface (or at least their components in the direction of the ferromagnetic moments deep within the FM layer, i.e., the direction of average magnetization $\hat{\mathbf{M}}$) are cut off at a mathematical interface, which we call the magnetic interface and which may not coincide with the chemical interface, either in its height fluctuations or over its average position, e.g., if a magnetic “dead layer” exists between the two interfaces (see Fig. 1). The disorder near the interface is thus represented by height fluctuations of this magnetic interface. The basis for this assumption, which is admittedly crude, is that the short (i.e., atomic) length-scale fluctuations of the moments away from the direction of the average magnetization give rise to diffuse scattering at fairly large scattering wave vectors, whereas we are dealing here with scattering at a small wave vector \mathbf{q} , which represent the relatively slow variations of the average magnetization density. The actual interface can be then considered as really composed of two interfaces, a chemical interface and a magnetic interface, each with their own average height, roughness, and correlation length, and, importantly, in general possessing correlated height fluctuations.

III. RESONANT MAGNETIC X-RAY SCATTERING AMPLITUDE

The amplitude for resonant magnetic scattering of x-rays has been derived by Hannon et al.,⁶ and a discussion of the general formalism may be found in the review by Hill and McMorrow.⁹ There are two cases of practical importance, namely dipole and quadrupole resonances. We shall restrict ourselves here to the most commonly used dipole resonance, which is related to the L-edges of transition metals and rare-earth atoms. The tensor amplitude for scattering $f_{\alpha\beta}$ from a magnetic atom is given by

$$\begin{aligned} \sum_{\alpha\beta} e_{f\alpha}^* f_{\alpha\beta} e_{i\beta} &= \left[f_0 + \frac{3\lambda}{8\pi} (F_{11} + F_{1-1}) \right] (\hat{\mathbf{e}}_f^* \cdot \hat{\mathbf{e}}_i) \\ &\quad - i \frac{3\lambda}{8\pi} (F_{11} - F_{1-1}) (\hat{\mathbf{e}}_f^* \times \hat{\mathbf{e}}_i) \cdot \hat{\mathbf{M}} \\ &\quad + \frac{3\lambda}{8\pi} (2F_{10} - F_{11} - F_{1-1}) (\hat{\mathbf{e}}_f^* \cdot \hat{\mathbf{M}}) (\hat{\mathbf{e}}_i \cdot \hat{\mathbf{M}}), \end{aligned} \quad (3.1)$$

where $\hat{\mathbf{e}}_i$, $\hat{\mathbf{e}}_f$ are, respectively, the unit photon polarization vectors for the incident and scattered waves, $\hat{\mathbf{M}}$ is a unit vector in the direction of the magnetic moment of the atom, λ is the x-ray photon wavelength, f_0 is the usual Thomson (charge) scattering amplitude [$f_0 = -r_0(Z + f' - if'')$], where r_0 is the Thomson scattering length (e^2/mc^2), Z is the atomic number, $f'(< 0)$ and $f''(> 0)$ are the real and imaginary non-resonant dispersion corrections. F_{LM} is the resonant scattering amplitude, as defined in Ref. 6, and has the resonant denominator $E_{\text{res}} - E - i\Gamma/2$, which provides the resonance when the photon energy E is tuned to the resonant energy E_{res} close to the absorption edges. The lifetime of the resonance Γ is typically 1 – 10 eV, so that the necessary energy resolution is easily achievable at synchrotron radiation beamlines. (We assumed that \mathbf{q} , the wave-vector transfer, is small enough here that the atomic form factor can be taken as unity.) Equation (3.1) has both real and imaginary (i.e., absorptive) components. The latter gives rise to the well-known phenomenon of x-ray magnetic circular or linear dichroism, whereas the real part gives rise to the scattering. Equation (3.1) yields

$$f_{\alpha\beta} = A\delta_{\alpha\beta} - iB \sum_{\gamma} \epsilon_{\alpha\beta\gamma} M_{\gamma} + CM_{\alpha}M_{\beta}, \quad (3.2)$$

where

$$A = f_0 + \frac{3\lambda}{8\pi} (F_{11} + F_{1-1}),$$

$$\begin{aligned}
B &= \frac{3\lambda}{8\pi}(F_{11} - F_{1-1}), \\
C &= \frac{3\lambda}{8\pi}(2F_{10} - F_{11} - F_{1-1}),
\end{aligned}
\tag{3.3}$$

and α, β denote Cartesian components, and $\epsilon_{\alpha\beta\gamma}$ is the antisymmetric Levi-Civita symbol ($\epsilon_{xyz} = \epsilon_{yzx} = \epsilon_{zxy} = 1$, $\epsilon_{xzy} = \epsilon_{yxz} = \epsilon_{zyx} = -1$, all other $\epsilon_{\alpha\beta\gamma} = 0$). The dielectric susceptibility of a resonant magnetic medium is given by

$$\chi_{\alpha\beta}^{\text{resonant}}(\mathbf{r}) = \frac{4\pi}{k_0^2} n_m(\mathbf{r}) f_{\alpha\beta}(\mathbf{r}),
\tag{3.4}$$

where $k_0 = 2\pi/\lambda$, $n_m(\mathbf{r})$ is the local number density of resonant magnetic atoms, and the variation of $f_{\alpha\beta}(\mathbf{r})$ with \mathbf{r} reflects the possible positional dependence of the direction of magnetization \mathbf{M} . The total dielectric susceptibility is given by

$$\begin{aligned}
\chi_{\alpha\beta}(\mathbf{r}) &= \frac{4\pi}{k_0^2} \left[\left\{ -\rho_0(\mathbf{r})r_0 + An_m(\mathbf{r}) \right\} \delta_{\alpha\beta} \right. \\
&\quad \left. - iBn_m(\mathbf{r}) \sum_{\gamma} \epsilon_{\alpha\beta\gamma} M_{\gamma}(\mathbf{r}) + Cn_m(\mathbf{r}) M_{\alpha}(\mathbf{r}) M_{\beta}(\mathbf{r}) \right],
\end{aligned}
\tag{3.5}$$

where $\rho_0(\mathbf{r})$ represents the electron number density arising from all the other nonresonant atoms in the medium modified by their anomalous dispersion corrections when necessary. Using the constitutive relationship between the local dielectric constant tensor $\epsilon_{\alpha\beta}(\mathbf{r})$ and $\chi_{\alpha\beta}(\mathbf{r})$,

$$\epsilon_{\alpha\beta}(\mathbf{r}) = \delta_{\alpha\beta} + \chi_{\alpha\beta}(\mathbf{r}).
\tag{3.6}$$

We note that the magnetization gives the dielectric tensor the same symmetry as in conventional magneto-optic theory, namely an antisymmetric component linear in the magnetization.

IV. THE DISTORTED-WAVE BORN APPROXIMATION FOR A SINGLE MAGNETIC INTERFACE

The results for specular reflectivity in the Born approximation (BA) have been derived in Ref. 19 and will be also summarized briefly in connection with the cross section in the following paper.²⁰ Here we discuss the scattering in terms of the distorted-wave Born approximation (DWBA). While this is more complicated algebraically, it provides a better

description than the simple kinematical approximation or BA in the vicinity of regions where total reflection or Bragg scattering occurs. This treatment is a generalization of that used in Ref. 17 for charge scattering. The wave equation for electromagnetic waves propagating in an anisotropic medium with a dielectric susceptibility tensor given by Eq. (3.5) may be written as

$$\sum_{\beta} [(\nabla^2 + k_0^2)\delta_{\alpha\beta} - \nabla_{\alpha}\nabla_{\beta} + k_0^2\chi_{\alpha\beta}] E_{\beta}(\mathbf{r}) = 0, \quad (\alpha, \beta = x, y, z), \quad (4.1)$$

where $\mathbf{E}(\mathbf{r})$ is the electric field vector.

Consider a wave incident, as in Fig. 1 with wave vector \mathbf{k}_i in the (x, z) plane ($k_{i,y} = 0$) and polarization μ ($\mu = \sigma$ or π), from a nonmagnetic (isotropic) medium for which $\chi_{\alpha\beta} = \chi_0\delta_{\alpha\beta}$ onto a smooth interface at $z = 0$ with a magnetic medium, for which $\chi_{\alpha\beta}$ is constant for $z < 0$.

Let us write for $z < 0$

$$\chi_{\alpha\beta} = \chi_1\delta_{\alpha\beta} + \chi_{\alpha\beta}^{(2)}, \quad (4.2)$$

where the term $\chi_{\alpha\beta}^{(2)}$ is the part that specifically depends on the magnetization \mathbf{M} , as defined in Eq. (3.5). The incident wave (chosen for convenience with unit amplitude) may be written as

$$\mathbf{E}_{\mu}^i(\mathbf{r}) = \hat{\mathbf{e}}_{\mu} e^{i\mathbf{k}_i \cdot \mathbf{r}}. \quad (4.3)$$

This incident wave will in general give rise to two specularly reflected waves (where the index μ refers to σ or π polarization) and two transmitted (refracted) waves in the magnetic medium. The complete solution for the electric field in the case of the smooth magnetic interface is then given by

$$\begin{aligned} \mathbf{E}_{(\mathbf{k}_i, \mu)}(\mathbf{r}) &= \hat{\mathbf{e}}_{\mu} e^{i\mathbf{k}_i \cdot \mathbf{r}} + \sum_{\nu=\sigma, \pi} R_{\nu\mu}^{(0)}(\mathbf{k}_i) \hat{\mathbf{e}}_{\nu} e^{i\mathbf{k}_i^r \cdot \mathbf{r}}, \quad z > 0, \\ &= \sum_{j=1,2} T_{j\mu}^{(0)}(\mathbf{k}_i) \hat{\mathbf{e}}_j e^{i\mathbf{k}_i^t(j) \cdot \mathbf{r}}, \quad z < 0, \end{aligned} \quad (4.4)$$

where \mathbf{k}_i^r is the specularly reflected wave vector in the nonmagnetic medium, ν denotes the polarization of the appropriate reflected component, the index $j(= 1, 2)$ defines the component of the transmitted wave in the magnetic resonant medium with polarization $\hat{\mathbf{e}}_j$ ($\hat{\mathbf{e}}_{j=1,2} = \hat{\mathbf{e}}^{(1)}$ and $\hat{\mathbf{e}}^{(2)}$, respectively, as defined in Appendix A), and $\mathbf{k}_i^t(j)$ the appropriate

wave vector for that transmitted wave. The polarization vectors $\hat{\mathbf{e}}$ may be real or complex allowing for linear or elliptically polarized waves. We denote such states in Eq. (4.4) quantum-mechanically by $|\mathbf{k}_i, \mu\rangle$.

$R_{\nu\mu}^{(0)}$ and $T_{j\mu}^{(0)}$ denote the appropriate reflection and transmission coefficients for the smooth surface and are expressed in terms of 2×2 matrices using the polarization bases for the incident and reflected (or transmitted) waves. The polarization basis is given by $(\hat{\mathbf{e}}_\sigma, \hat{\mathbf{e}}_\pi)$, as shown in Fig. 1, for the waves in the nonmagnetic medium and $(\hat{\mathbf{e}}^{(1)}, \hat{\mathbf{e}}^{(2)})$, as defined in Appendix A, for those in the magnetic resonant medium, respectively. The convention in which the polarization state of the reflected (or transmitted) wave precedes that of the incident wave is used for the subscripts in $R_{\nu\mu}^{(0)}$ and $T_{j\mu}^{(0)}$, and the Greek and Roman letters are used for the polarization states in the nonmagnetic and magnetic medium, respectively. The explicit expressions of $R_{\nu\mu}^{(0)}$ and $T_{j\mu}^{(0)}$ for small angles of incidence and small amplitudes of the dielectric susceptibility and for special directions of the polarization and magnetization (i.e., $\mathbf{M} \parallel \hat{\mathbf{x}}$ as shown in Fig. 1) are given in Appendix A.

We should mention, however, that these specific conditions considered in Appendix A (and also in all other appendices) are reasonably satisfied for hard- and medium-energy x-rays and also for soft x-rays around transition-metal L-edges with small angles (i.e., when $\theta_i^2 \ll 1$ for the incidence angle θ_i). We should also mention that, even when \mathbf{M} is not parallel to the $\hat{\mathbf{x}}$ -axis in Fig. 1, the expressions derived in the appendices can be still applied by considering only the x -component of the magnetization vector \mathbf{M} . This is because the y - and z -components of \mathbf{M} contribute negligibly to the scattering in comparison with the dominant factor $B = (3\lambda/8\pi)(F_{11} - F_{1-1})$ in Eq. (3.2) at small angles¹⁵ when $|F_{11} - F_{1-1}| \gg |2F_{10} - F_{11} - F_{1-1}|$, which is generally satisfied for transition-metal and rare-earth L-edges.⁸

We note that the continuity of the fields parallel to the interface requires that

$$(\mathbf{k}_i)_\parallel = (\mathbf{k}_i^r)_\parallel = (\mathbf{k}_i^t(j))_\parallel, \quad (4.5)$$

where $(\)_\parallel$ denotes the vector component parallel to the interface.

We now discuss the structurally and magnetically rough interface. For this purpose we shall assume that the average height (along z) of the structural and magnetic interfaces is the same, i.e., we ignore the presence of a magnetic dead layer. This may be treated within the DWBA as simply another nonmagnetic layer and thus discussed within the formalism

for treating multilayers as discussed in Section VII. We can write

$$\chi_{\alpha\beta}(\mathbf{r}) = \chi_{\alpha\beta}^{(0)}(\mathbf{r}) + \Delta_{\alpha\beta}^c(\mathbf{r}) + \Delta_{\alpha\beta}^m(\mathbf{r}), \quad (4.6)$$

where

$$\begin{aligned} \chi_{\alpha\beta}^{(0)}(\mathbf{r}) &= \chi_0 \delta_{\alpha\beta}, \quad z > 0 \\ &= \chi_1 \delta_{\alpha\beta} + \chi_{\alpha\beta}^{(2)}, \quad z < 0, \end{aligned} \quad (4.7)$$

$$\begin{aligned} \Delta_{\alpha\beta}^c(\mathbf{r}) &= (\chi_1 - \chi_0) \delta_{\alpha\beta}, \quad \text{for } 0 < z < \delta z_c(x, y) \text{ if } \delta z_c(x, y) > 0 \\ &= -(\chi_1 - \chi_0) \delta_{\alpha\beta}, \quad \text{for } \delta z_c(x, y) < z < 0 \text{ if } \delta z_c(x, y) < 0 \\ &= 0 \quad \text{elsewhere,} \end{aligned} \quad (4.8)$$

and

$$\begin{aligned} \Delta_{\alpha\beta}^m(\mathbf{r}) &= \chi_{\alpha\beta}^{(2)}, \quad \text{for } 0 < z < \delta z_m(x, y) \text{ if } \delta z_m(x, y) > 0 \\ &= -\chi_{\alpha\beta}^{(2)}, \quad \text{for } \delta z_m(x, y) < z < 0 \text{ if } \delta z_m(x, y) < 0 \\ &= 0 \quad \text{elsewhere,} \end{aligned} \quad (4.9)$$

$\delta z_c(x, y)$ and $\delta z_m(x, y)$ define the structural (chemical) and magnetic interfaces, respectively.

We may also define the time-reversed function corresponding to a wave incident on the interface with vector $(-\mathbf{k}_f)$ and polarization ν as

$$\begin{aligned} \mathbf{E}_{(-\mathbf{k}_f, \nu)}^T(\mathbf{r}) &= \hat{\mathbf{e}}_\nu e^{i\mathbf{k}_f^* \cdot \mathbf{r}} + \sum_{\lambda=\sigma, \pi} R_{\lambda\nu}^{(0)*}(-\mathbf{k}_f) \hat{\mathbf{e}}_\lambda e^{i\mathbf{k}_f^* \cdot \mathbf{r}}, \quad z > 0 \\ &= \sum_{j=1,2} T_{j\nu}^{(0)*}(-\mathbf{k}_f) \hat{\mathbf{e}}_j e^{i\mathbf{k}_f^{t*}(j) \cdot \mathbf{r}}, \quad z < 0, \end{aligned} \quad (4.10)$$

where $(-\mathbf{k}_f^r)$ is the wave vector of the wave specularly reflected from $(-\mathbf{k}_f)$, and $(-\mathbf{k}_f^t(j))$ is the wave vector of one of the two transmitted waves in the medium emanating from $(-\mathbf{k}_f)$ incident on the surface, as shown in Fig. 2. Note that, for consistency with the conventions used in Eq. (4.4), the polarization vectors in Eq. (4.10) are defined in the ordinary coordinate system where their phases are considered along the left-to-right direction in Fig. 1. Otherwise, the polarization vectors in Eq. (4.10) should be replaced by their complex conjugates.

We have also the conditions

$$(\mathbf{k}_f)_\parallel = (\mathbf{k}_f^r)_\parallel = (\mathbf{k}_f^t(j))_\parallel. \quad (4.11)$$

The DWBA then yields the differential cross section for scattering by the rough interface from (\mathbf{k}_i, μ) to (\mathbf{k}_f, ν) as

$$\frac{d\sigma}{d\Omega} = \frac{1}{16\pi^2} \langle |\mathcal{T}^{fi}|^2 \rangle, \quad (4.12)$$

where $\mathcal{T}^{fi} = \langle \mathbf{k}_f, \nu | \mathcal{T} | \mathbf{k}_i, \mu \rangle$ is the scattering matrix element, and $\langle \dots \rangle$ in Eq. (4.12) denotes a statistical averaging over random fluctuations at the interface. Following Ref. 17, we split the cross section into two parts:

$$\frac{d\sigma}{d\Omega} = \frac{1}{16\pi^2} |\langle \mathcal{T}^{fi} \rangle|^2 + \frac{1}{16\pi^2} \left[\langle |\mathcal{T}^{fi}|^2 \rangle - |\langle \mathcal{T}^{fi} \rangle|^2 \right]. \quad (4.13)$$

The first term in Eq. (4.13) represents the coherent (specular) part of the scattering, which corresponds to a statistical averaging of the scattering amplitude, and the second term corresponds to the incoherent (diffuse) scattering. In this paper, we shall deal with the first term only, while the diffuse scattering will be addressed in the following paper.²⁰

The DWBA consists of approximating the scattering matrix element by the expression

$$\begin{aligned} \langle \mathbf{k}_f, \nu | \mathcal{T} | \mathbf{k}_i, \mu \rangle &= k_0^2 \langle -\mathbf{k}_f^T, \nu | \boldsymbol{\chi}^{(0)} | \mathbf{E}_\mu^i(\mathbf{r}) \rangle \\ &+ k_0^2 \langle -\mathbf{k}_f^T, \nu | \boldsymbol{\Delta}^c | \mathbf{k}_i, \mu \rangle + k_0^2 \langle -\mathbf{k}_f^T, \nu | \boldsymbol{\Delta}^m | \mathbf{k}_i, \mu \rangle. \end{aligned} \quad (4.14)$$

Here $|\mathbf{E}_\mu^i(\mathbf{r}) \rangle$ denotes the “pure” incoming wave in Eq. (4.3), $|-\mathbf{k}_f^T, \nu \rangle$ denotes the state in Eq. (4.10), and the matrix element involves dot products of the tensor operators $\boldsymbol{\chi}^{(0)}$, $\boldsymbol{\Delta}^c$, and $\boldsymbol{\Delta}^m$ with the vector fields $\langle -\mathbf{k}_f^T, \nu |$ and $\langle \mathbf{k}_i, \mu |$. While $\boldsymbol{\chi}^{(0)}$ represents an ideal system with a smooth interface, $\boldsymbol{\Delta}^c$ and $\boldsymbol{\Delta}^m$ are perturbations on $\boldsymbol{\chi}^{(0)}$ due to interface roughnesses.

For the smooth surface, only the first tensor is nonvanishing, and, following Ref. 17, we can show from Eqs. (4.3) and (4.10) that

$$\begin{aligned} k_0^2 \langle -\mathbf{k}_f^T, \nu | \boldsymbol{\chi}^{(0)} | \mathbf{E}_\mu^i(\mathbf{r}) \rangle &= i\mathcal{A}k_0^2 \delta_{k_{ix}k_{fx}} \delta_{k_{iy}k_{fy}} \\ &\times \sum_j T_{j\nu}^{(0)}(-\mathbf{k}_f) \sum_{\alpha\beta} e_{j\alpha}^* (\chi_1 \delta_{\alpha\beta} + \chi_{\alpha\beta}^{(2)}) e_{\mu\beta} \\ &\times \int_{-\infty}^0 dz e^{-i(k_{fz}^t(j) - k_{iz})z}, \\ &= 2i\mathcal{A}k_{iz} R_{\nu\mu}^{(0)}(\mathbf{k}_i) \delta_{k_{ix}k_{fx}} \delta_{k_{iy}k_{fy}}, \end{aligned} \quad (4.15)$$

where \mathcal{A} is the illuminated surface area, and $R_{\nu\mu}^{(0)}(\mathbf{k}_i)$ is the reflection coefficient for the smooth surface, as defined in Eq. (4.4). The details of Eq. (4.15) are presented in Appendix

B. By comparison with Eq. (4.15) for the smooth surface, the scattering matrix element for the rough surface in Eq. (4.14) can be analogously defined by

$$\langle \mathbf{k}_f, \nu | \mathcal{T} | \mathbf{k}_i, \mu \rangle = 2i\mathcal{A}k_{iz}R_{\nu\mu}(\mathbf{k}_i)\delta_{k_{ix}k_{fx}}\delta_{k_{iy}k_{fy}}, \quad (4.16)$$

where $R_{\nu\mu}(\mathbf{k}_i)$ denotes the reflection coefficient for the rough surface.

On the other hand, for the reverse case where a wave is incident from a resonant magnetic medium to a nonmagnetic (isotropic) medium, similarly to Eq. (4.15), the scattering matrix element for the smooth surface can be shown to be

$$k_0^2 \langle -\mathbf{k}_f^T, j' | \mathcal{X}^{(0)} | \mathbf{k}_i, j \rangle = 4i\mathcal{A}k_{iz}(j)R_{j'j}^{(0)}(\mathbf{k}_i)\delta_{k_{ix}k_{fx}}\delta_{k_{iy}k_{fy}}, \quad (4.17)$$

where the incoming wave from the resonant magnetic medium $|\mathbf{k}_i, j \rangle$ is used instead of the “pure” incoming wave from the vacuum $\mathbf{E}_\mu^i(\mathbf{r})$ in Eq. (4.3). The use of Eqs. (4.15) and (4.17) in Eqs. (4.14) and (4.12) in the case of the smooth surface and the derivation of the corresponding reflectivity in the usual manner, as discussed in Ref. 17, shows that Eqs. (4.15) and (4.17) must be identically true. Similarly to Eqs. (4.15) and (4.16), the scattering matrix element for the rough surface between reversed layers can be also defined by analogy from Eq. (4.17) as

$$\langle \mathbf{k}_f, j' | \mathcal{T} | \mathbf{k}_i, j \rangle = 4i\mathcal{A}k_{iz}(j)R_{j'j}(\mathbf{k}_i)\delta_{k_{ix}k_{fx}}\delta_{k_{iy}k_{fy}}, \quad (4.18)$$

where $R_{j'j}(\mathbf{k}_i)$ denotes the reflection coefficient for the rough surface between reversed layers.

V. REFLECTION AND TRANSMISSION COEFFICIENTS USING THE SELF-CONSISTENT METHOD

To calculate specular reflectivity, we make an approximation in the spirit of Nevot and Croce.²¹ To evaluate the matrix elements in Eq. (4.14) involving $\Delta_{\alpha\beta}^c$ and $\Delta_{\alpha\beta}^m$, we assume for $\mathbf{E}(\mathbf{k}_i, \mu)$ in Eq. (4.4) the functional form for $z > 0$ analytically continued for $z < 0$, while for the time-reversed state $\mathbf{E}^T(-\mathbf{k}_f, \nu)$ in Eq. (4.10) the functional form for $z < 0$ analytically continued to $z > 0$. Then, bearing in mind that for specular reflectivity $\mathbf{k}_f = \mathbf{k}_i^r$ and using Eq. (4.5), we obtain for the statistically averaged amplitude $\langle \mathcal{T}^{fi} \rangle$:

$$\langle k_0^2 \langle -\mathbf{k}_f^T, \nu | \Delta^{c,m} | \mathbf{k}_i, \mu \rangle \rangle = i\mathcal{A}k_0^2 \sum_{j=1,2} T_{j\nu}^{(0)}(-\mathbf{k}_f)$$

$$\begin{aligned}
& \times \left[\sum_{\alpha\beta} \frac{e_{j\alpha}^* \Delta_{\alpha\beta}^{c,m} e_{\mu\beta}}{q_{1z}(j)} \left[\langle e^{-iq_{1z}(j)\delta z_{c,m}(x,y)} \rangle - 1 \right] \right. \\
& \left. + \sum_{\lambda=\sigma,\pi} R_{\lambda\mu}^{(0)}(\mathbf{k}_i) \sum_{\alpha\beta} \frac{e_{j\alpha}^* \Delta_{\alpha\beta}^{c,m} e_{\lambda\beta}}{q_{2z}(j)} \left[\langle e^{-iq_{2z}(j)\delta z_{c,m}(x,y)} \rangle - 1 \right] \right], \quad (5.1)
\end{aligned}$$

where

$$q_{1z}(j) = k_{fz}^t(j) - k_{iz}, \quad q_{2z}(j) = k_{fz}^t(j) - k_{iz}^r, \quad (5.2)$$

and $\Delta_{\alpha\beta}^{c,m}$ is the value defined for $0 < z < \delta z_{c,m}$ in Eqs. (4.8) and (4.9). From Eqs. (4.15)-(4.16) and (5.1), we see that, at the specular condition, we can write Eq. (4.14) as

$$R_{\nu\mu} = R_{\nu\mu}^{(0)} + U_{\nu\mu} + \sum_{\lambda} V_{\nu\lambda} R_{\lambda\mu}^{(0)}, \quad (5.3)$$

where

$$\begin{aligned}
U_{\nu\mu} = & \sum_{j=1,2} \frac{T_{j\nu}^{(0)}(-\mathbf{k}_f)}{2k_{iz}} \frac{k_0^2}{q_{1z}(j)} \left[(\chi_1 - \chi_0) \sum_{\alpha} e_{j\alpha}^* e_{\mu\alpha} [e^{-\frac{1}{2}q_{1z}^2(j)\sigma_c^2} - 1] \right. \\
& \left. + \sum_{\alpha\beta} e_{j\alpha}^* \chi_{\alpha\beta}^{(2)} e_{\mu\beta} [e^{-\frac{1}{2}q_{1z}^2(j)\sigma_m^2} - 1] \right], \quad (5.4)
\end{aligned}$$

and replacing q_{1z} , e_{μ} in $U_{\nu\mu}$ by q_{2z} , e_{λ} produces $V_{\nu\lambda}$. Here we made the customary Gaussian approximation for the height fluctuations $\delta z_{c,m}(x, y)$, and σ_c , σ_m are the root-mean-squared structural and magnetic roughnesses, respectively. Note that the correlation term $U_{\nu\mu}$ due to the roughness in the reflection coefficient contains only independent contributions of chemical and magnetic roughnesses expressed via σ_c and σ_m , respectively. According to Eq. (4.13), the diffuse scattering must contain the cross-correlation component due to the term $\langle |\mathcal{T}^{fi}|^2 \rangle$.

A better approximation than Eq. (5.3) may be obtained by using the rough-interface reflection coefficient $R_{\nu\mu}$ instead of the smooth-interface $R_{\nu\mu}^{(0)}$ in the wave functions of Eqs. (4.4) and (4.10), thus getting a self-consistent matrix equation in terms of the 2×2 matrices, \mathbf{R} , \mathbf{U} , \mathbf{V} . This leads to

$$\mathbf{R} = \mathbf{R}^{(0)} + \mathbf{U} + \mathbf{V}\mathbf{R}, \quad (5.5)$$

whose solution is

$$\mathbf{R} = (\mathbf{1} - \mathbf{V})^{-1}(\mathbf{R}^{(0)} + \mathbf{U}). \quad (5.6)$$

Similarly, for the reverse interface between upper resonant magnetic and lower nonmagnetic layers, we can have the same solution as Eq. (5.6) from Eqs. (4.17) and (4.18). The explicit expressions of \mathbf{U} , \mathbf{V} , $\mathbf{R}^{(0)}$ matrices in Eq. (5.6) for both cases are given in Appendix C.

For nonmagnetic interfaces, the matrices are all diagonal (σ and π polarizations are decoupled), and it has been shown that Eq. (5.6) leads to the familiar Nevot-Croce form²¹ for the reflection coefficient, i.e.,

$$R = R^{(0)} e^{-2|k_z||k_z^t|\sigma_c^2}. \quad (5.7)$$

The derivation of this is shown in Appendix D. For the magnetic interface, this simplified form for the reflection coefficient does not have any analogue. Nevertheless, at sufficiently large values of q_z , the reflectivity takes the familiar Gaussian form $R^{(0)} e^{-q_z^2 \sigma_{\text{eff}}^2}$. However, σ_{eff}^2 does not always take the form predicted by the simple kinematical theory [i.e., σ_c^2 for $\sigma \rightarrow \sigma$ reflectivity, σ_m^2 for $\sigma \rightarrow \pi$ reflectivity, and $\frac{1}{2}(\sigma_c^2 + \sigma_m^2)$ for $(I_+ - I_-)$ in the case of circularly polarized x-rays] as we shall see in the numerical example shown below, which provides a counter-illustration of the rule that, at large q_z , the DWBA becomes identical to the Born approximation or kinematical limit.

For circularly polarized incident x-rays with $\hat{\mathbf{e}}_{\pm}(\vec{k}_i) = (\hat{\mathbf{e}}_{\sigma}(\vec{k}_i) \pm i\hat{\mathbf{e}}_{\pi}(\vec{k}_i)) / \sqrt{2}$, the reflection amplitudes for σ - and π -polarization are given by

$$\begin{pmatrix} R_{\sigma} \\ R_{\pi} \end{pmatrix} = \mathbf{R} \begin{pmatrix} \frac{1}{\sqrt{2}} \\ \pm \frac{i}{\sqrt{2}} \end{pmatrix}, \quad (5.8)$$

where \mathbf{R} is the 2×2 matrix reflection coefficient in Eq. (5.6). The reflected intensities without polarization analysis for the outgoing beam, $I = \sqrt{|R_{\sigma}|^2 + |R_{\pi}|^2}$, can be then evaluated for the opposite helicities of incident beams as

$$I_+ - I_- = 2 \text{Im}[R_{11}R_{12}^* + R_{21}R_{22}^*], \quad (5.9)$$

where R_{ij} is the ij -element of the 2×2 matrix \mathbf{R} .

Since Parratt's recursive formula for multiple interfaces includes only reflection coefficients, its extension to the rough interface case does not need the transmission coefficient to account for interface roughness. On the other hand, in our case where the fields are not scalars, the transmission coefficients are requisite to calculate recursive 2×2 matrix formulae for multiple magnetic interfaces, which will be discussed in Sec. VII. For completeness,

therefore, let us now calculate the transmission coefficient $T_{j\mu}$ from a rough interface. In the spirit of Ref. 22, we assume for $\mathbf{E}(\mathbf{k}_i, \mu)$ and $\mathbf{E}^T(-\mathbf{k}_f, j)$ the functional forms analytically continued both for $z > 0$ and for $z < 0$ as follows:

$$\mathbf{E}(\mathbf{k}_i, \mu) = \sum_{j'=1,2} T_{j'\mu}^{(0)}(\mathbf{k}_i) \hat{\mathbf{e}}_{j'} e^{i\mathbf{k}_i^t(j') \cdot \mathbf{r}}, \quad (5.10)$$

$$\mathbf{E}^T(-\mathbf{k}_f, j) = \sum_{\nu=\sigma,\pi} T_{\nu j}^{(0)*}(-\mathbf{k}_f) \hat{\mathbf{e}}_{\nu} e^{-i\mathbf{k}_f^* \cdot \mathbf{r}}, \quad (5.11)$$

where $T_{\nu j}^{(0)*}(-\mathbf{k}_f)$ in Eq. (5.11) denotes the transmission coefficient “from” a magnetic(anisotropic) medium “to” a nonmagnetic (isotropic) one, whose explicit form is given in Appendix A. For the smooth surface, the scattering matrix element between the eigenstates $|-\mathbf{k}_f^T, j\rangle$ and $|\mathbf{k}_i, \mu\rangle$ can be then written as

$$\begin{aligned} k_0^2 \langle -\mathbf{k}_f^T, j | \chi^{(0)} | \mathbf{k}_i, \mu \rangle &= i\mathcal{A}k_0^2 \delta_{k_{ix}k_{fx}} \delta_{k_{iy}k_{fy}} \\ &\times \sum_{\nu} T_{\nu j}^{(0)}(-\mathbf{k}_f) \sum_{j'} T_{j'\mu}^{(0)}(\mathbf{k}_i) \sum_{\alpha\beta} e_{\nu\alpha}^* (\chi_1 \delta_{\alpha\beta} + \chi_{\alpha\beta}^{(2)}) e_{j'\beta} \\ &\times \int_{-\infty}^0 dz e^{-i(-k_{fz} - k_{iz}^t(j'))z}, \\ &= 4i\mathcal{A}k_{iz}^t(j) T_{j\mu}^{(0)}(\mathbf{k}_i) \delta_{k_{ix}k_{fx}} \delta_{k_{iy}k_{fy}}, \end{aligned} \quad (5.12)$$

where $T_{j\mu}^{(0)}(\mathbf{k}_i)$ is the transmission coefficient for the smooth surface, as defined in Eq. (4.4). The details of Eqs. (5.12) are given in Appendix B.

In comparison with Eq. (5.12) for the smooth surface, the scattering matrix element for the rough surface, as shown in Eq. (4.14), can be analogously defined by

$$\langle \mathbf{k}_f, j | \mathcal{T} | \mathbf{k}_i, \mu \rangle = 4i\mathcal{A}k_{iz}^t(j) T_{j\mu}(\mathbf{k}_i) \delta_{k_{ix}k_{fx}} \delta_{k_{iy}k_{fy}}, \quad (5.13)$$

where $T_{j\mu}(\mathbf{k}_i)$ denotes the transmission coefficient for the rough surface.

For the statistically averaged amplitude $\langle \mathcal{T}^{fi} \rangle$, we obtain

$$\begin{aligned} \langle k_0^2 \langle -\mathbf{k}_f^T, j | \Delta^{c,m} | \mathbf{k}_i, \mu \rangle \rangle &= i\mathcal{A}k_0^2 \sum_{\nu} T_{\nu j}^{(0)}(-\mathbf{k}_f) \\ &\times \sum_{j'} T_{j'\mu}^{(0)}(\mathbf{k}_i) \sum_{\alpha\beta} \frac{e_{\nu\alpha}^* \Delta_{\alpha\beta}^{c,m} e_{j'\beta}}{q_{3z}(j')} \left[\langle e^{-iq_{3z}(j')\delta z_{c,m}(x,y)} \rangle - 1 \right] \end{aligned} \quad (5.14)$$

and

$$q_{3z}(j') = -k_{fz} - k_{iz}^t(j'). \quad (5.15)$$

From Eqs. (5.12)-(5.13) and (5.14), we see that we can write the scattering matrix element in the DWBA, as shown in Eq. (4.14), as

$$T_{j\mu} = T_{j\mu}^{(0)} + \sum_{j'=1,2} V'_{jj'} T_{j'\mu}^{(0)}, \quad (5.16)$$

where

$$V'_{jj'} = \sum_{\nu} \frac{T_{\nu j}^{(0)}(-\mathbf{k}_f)}{4k_{iz}^t(j)} \frac{k_0^2}{q_{3z}(j')} \left[(\chi_1 - \chi_0) \sum_{\alpha} e_{\nu\alpha}^* e_{j'\alpha} \left[e^{-\frac{1}{2}q_{3z}^2(j')\sigma_c^2} - 1 \right] + \sum_{\alpha\beta} e_{\nu\alpha}^* \chi_{\alpha\beta}^{(2)} e_{j'\beta} \left[e^{-\frac{1}{2}q_{3z}^2(j')\sigma_m^2} - 1 \right] \right]. \quad (5.17)$$

In the same way as we did for the reflection coefficient, using the rough-interface transmission coefficient $T_{j\mu}$ instead of the smooth-interface $T_{j\mu}^{(0)}$ in the right side of Eq. (5.16), thus getting a self-consistent matrix equation in terms of the 2×2 matrices, \mathbf{T} , \mathbf{V}' , gives

$$\mathbf{T} = \mathbf{T}^{(0)} + \mathbf{V}'\mathbf{T}, \quad (5.18)$$

whose solution is

$$\mathbf{T} = (\mathbf{1} - \mathbf{V}')^{-1} \mathbf{T}^{(0)}. \quad (5.19)$$

Similarly, for the reverse interface between upper resonant magnetic and lower nonmagnetic layers, we can also have the same solution as Eq. (5.19). The explicit expressions of \mathbf{V}' and $\mathbf{T}^{(0)}$ matrices in Eq. (5.19) for both cases are given in Appendix C.

For nonmagnetic interfaces, it is shown in Appendix D that Eq. (5.19) reduces to

$$T = T^{(0)} e^{\frac{1}{2}(|k_z| - |k_z^t|)^2 \sigma_c^2}, \quad (5.20)$$

which has been found by Vidal and Vincent.²³

VI. NUMERICAL EXAMPLES FOR A SINGLE MAGNETIC SURFACE

We now illustrate numerical examples of the above formulae calculated for a Gd surface with varying degrees of structural and magnetic roughness. We have considered only the case where the magnetization vector is aligned along the sample surface in the scattering plane in order to enhance the magnetic effect.

Figure 3 shows the x-ray resonant magnetic reflectivities calculated at the Gd L₃-edge (7243 eV) from Gd surfaces with different interfacial widths for structural (σ_c) and magnetic

(σ_m) interfaces. In Fig. 3(a)-(c), the interfacial width of the structural interface is larger than that of the magnetic interface, that is, $\sigma_c = 8 \text{ \AA}$ and $\sigma_m = 3 \text{ \AA}$. On the other hand, in Fig. 3(d)-(f), the interfacial widths are reversed, that is, $\sigma_c = 3 \text{ \AA}$ and $\sigma_m = 8 \text{ \AA}$. In the kinematical approximation(BA) $\sigma \rightarrow \sigma$ scattering (solid lines in the top panels of Fig. 3) corresponds to pure charge scattering, and $\sigma \rightarrow \pi$ scattering (dashed lines in the top panels of Fig. 3) to pure magnetic scattering, and the differences between the reflected intensities for right- (I_+) and left- (I_-) circularly polarized incident beams (circles in Fig. 3) correspond to the interferences between charge and magnetic scattering.

Kinematically, the reflected intensities from each scattering channels are proportional to a simple Gaussian form, $\exp(-\sigma^2 q_z^2)$, where σ is the interfacial width of corresponding scattering channel, i.e., σ_c for $I_{\sigma \rightarrow \sigma}$, σ_m for $I_{\sigma \rightarrow \pi}$, and $\sqrt{(\sigma_c^2 + \sigma_m^2)/2}$ for $(I_+ - I_-)$. The middle panel of Fig. 3 shows natural logarithms of the reflectivities from rough interfaces normalized to those from ideal systems without roughness as a function of the square of the wave vector, q_z^2 , whose slopes are then equal to the squares of the interfacial widths for their corresponding scattering channels. In Fig. 3(b), the slopes obtained from our dynamical calculation for the case of $\sigma_c = 8 \text{ \AA}$ and $\sigma_m = 3 \text{ \AA}$ show good agreement with the kinematical results mentioned above. On the other hand, in Fig. 3(e), the slopes of $I_{\sigma \rightarrow \pi}$ and $(I_+ - I_-)$ for the opposite case, $\sigma_c = 3 \text{ \AA}$ and $\sigma_m = 8 \text{ \AA}$, are not equal to the squares of their corresponding interfacial widths but follow the slope of $I_{\sigma \rightarrow \sigma}$ at high q_z 's.

This indicates that the kinematical argument mentioned above, i.e., one-to-one correspondence such as $\sigma \rightarrow \pi$ channel to pure magnetic scattering, is no longer valid for such a case of larger magnetic interfacial width, as shown in Fig. 3(e). In other words, both contributions from charge and magnetic scattering should be taken into account for every scattering channel, which is naturally included in the dynamical theory (such as our self-consistent method). In the case shown in Fig. 3(e), since the charge-scattering channel is much stronger than the magnetic-scattering channel and also drops off much more slowly with q_z due to decreased roughness, there is conversion of $\sigma \rightarrow \pi$ polarization at larger q_z even when the ‘‘pure’’ magnetic scattering has become negligible in the kinematical limit, because of magnetic scattering out of the still strong charge channel. Thus the $\sigma \rightarrow \pi$ and $(I_+ - I_-)$ reflections will asymptotically decay at a rate governed by the decay of the charge channel, which is determined by σ_c alone.

However, it is not easy to find a physical system where a magnetic interfacial width is

larger than the structural one at the same interface, as shown in Fig. 3(f). Instead, such a rougher magnetic interface can occur in a magnetic system, where a magnetically “dead” layer exists near the top surface and so the average position of the magnetic interface may not coincide with that of the structural interface, as shown in Fig. 3(i). In Fig. 3(g) ($I_+ - I_-$) (circles) shows an oscillation due to a magnetically dead layer with its thickness of 20 Å. In this case, the slopes in Fig. 3(h) follow again the kinematical result mentioned above because the magnetic interface and the structural one are separated spatially.

As a further check on our calculations, we have calculated the reflectivity by dividing the error-function profile, as shown in the bottom panel of Fig. 3, into many very thin slices and using the 2×2 recursive matrix formulae without any roughness assumptions.¹⁵ We found that the results using this slice method are exactly the same as those from our self-consistent method assuming Gaussian height distributions in Fig. 3. Thus our self-consistent method based on the DWBA produces very accurate results for the x-ray resonant magnetic reflectivity and much faster computationally.

VII. MULTIPLE MAGNETIC INTERFACES

For a multilayer with multiple interfaces, each layer can be characterized by its dielectric susceptibility tensor $\chi_{\alpha\beta,n}$ for the n -th layer, which can be $\chi_{\alpha\beta,n} = \chi_n \delta_{\alpha\beta}$ for nonmagnetic (isotropic) layers and $\chi_{\alpha\beta,n} = \chi_n \delta_{\alpha\beta} + \chi_{\alpha\beta,n}^{(2)}$ for magnetic (anisotropic) layers. For each rough interface, we can use the self-consistent DWBA to define the reflection and transmission coefficients, in the same way as in Sec. V, which are given by

$$\begin{aligned} \mathbf{R}_n &= (\mathbf{I} - \mathbf{V}_n)^{-1}(\mathbf{R}_n^{(0)} + \mathbf{U}_n) = \tilde{M}_n^{rt}, \\ \mathbf{T}_n &= (\mathbf{I} - \mathbf{V}'_n)^{-1}\mathbf{T}_n^{(0)} = \tilde{M}_n^{tt}, \end{aligned} \quad (7.1)$$

where \mathbf{R}_n , \mathbf{T}_n are the reflection and transmission coefficients for the n -th rough interface, and $\mathbf{R}_n^{(0)}$, $\mathbf{T}_n^{(0)}$ are those for the corresponding smooth interface. The explicit expressions for $\mathbf{R}_n^{(0)}$, $\mathbf{T}_n^{(0)}$, \mathbf{U}_n , \mathbf{V}_n , and \mathbf{V}'_n matrices in Eq. (7.1) are given in Appendix C, depending on whether the upper and lower layers on the n -th interface are nonmagnetic or magnetic layers, respectively.

By analogy with the recursion relation for the coupled waves derived for the smooth interfaces in Appendix E (originally developed by Stepanov and Sinha¹⁵), introducing \tilde{W}^{pq}

matrices for the rough interfaces, we may derive the recursion relation analogous to Eq. (E5), obtaining

$$\begin{aligned}
\tilde{W}_{n+1}^{tt} &= \tilde{A}_n \tilde{W}_n^{tt}, \\
\tilde{W}_{n+1}^{tr} &= \tilde{M}_{n+1}^{tr} + \tilde{A}_n \tilde{W}_n^{tr} \tilde{M}_{n+1}^{rr}, \\
\tilde{W}_{n+1}^{rt} &= \tilde{W}_n^{rt} + \tilde{B}_n \tilde{M}_{n+1}^{rt} \tilde{W}_n^{tt}, \\
\tilde{W}_{n+1}^{rr} &= \tilde{B}_n \tilde{M}_{n+1}^{rr},
\end{aligned} \tag{7.2}$$

where \tilde{A}_n and \tilde{B}_n are defined by

$$\begin{aligned}
\tilde{A}_n &= \tilde{M}_{n+1}^{tt} \left(1 - \tilde{W}_n^{rt} \tilde{M}_{n+1}^{rt}\right)^{-1}, \\
\tilde{B}_n &= \tilde{W}_n^{rr} \left(1 - \tilde{M}_{n+1}^{rt} \tilde{W}_n^{tr}\right)^{-1}.
\end{aligned} \tag{7.3}$$

Finally, the specular reflectivity of a magnetic multilayer with rough interfaces can be obtained by

$$R_0 = \tilde{W}_N^{rt} T_0. \tag{7.4}$$

To calculate the sum and difference in the reflectivities for (+) and (−) circularly polarized incident x-rays, substituting $T_0 = \frac{1}{\sqrt{2}}(1, \pm i)$ in a similar way to Eqs. (5.8) and (5.9) yields

$$\begin{aligned}
I_+ + I_- &= |(\tilde{W}_N^{rt})_{11}|^2 + |(\tilde{W}_N^{rt})_{12}|^2 + |(\tilde{W}_N^{rt})_{21}|^2 + |(\tilde{W}_N^{rt})_{22}|^2, \\
I_+ - I_- &= 2 \operatorname{Im} \left[(\tilde{W}_N^{rt})_{11} (\tilde{W}_N^{rt})_{12}^* + (\tilde{W}_N^{rt})_{21} (\tilde{W}_N^{rt})_{22}^* \right],
\end{aligned} \tag{7.5}$$

where $(\tilde{W}_N^{rt})_{ij}$ is the ij -element of the 2×2 matrix \tilde{W}_N^{rt} .

The above suggested approach to calculating the effects of roughness in multilayers on specular reflectivity is an approximation analogous to those used previously in several publications on charge-only roughness.^{18,24–26} Basically, it corresponds to averaging the reflection coefficient (or the scattering matrix) of each interface over the interface roughness. The comparison with the results of rigorous “slicing method” made in Ref. 26 has proven that such an approximation works very well. A possible reason for the excellent validity of this approximation is that the roughness effect is mainly displayed at greater incidence angles, where the reflection is small and the multiple scattering can be neglected (the total reflection amplitude is a linear sum of contributions from individual interfaces). Note that, since we are considering the coherent scattering which involves only the statistical average of the scattering amplitude in Eq. (4.13), there is no contribution from any cross-interface correlations of roughness. This will not be the case with diffuse (off-specular) scattering.²⁰

VIII. NUMERICAL EXAMPLES FOR MULTIPLE INTERFACES

We present here numerical examples for x-ray resonant magnetic reflectivity from a Gd/Fe multilayer using the above formulae. Since Gd/Fe multilayers (MLs) have vastly different Curie temperatures and strong interfacial coupling of Gd and Fe, these systems give rise to complex magnetic structures depending on the layer thickness, temperature, and applied magnetic field.²⁷ Due to the advantage of Gd L-edge resonances available in the hard x-ray regime, several experimental studies from these Gd/Fe MLs have been performed using x-ray resonant magnetic reflectivity measurements.^{13,14,28} Again, we have considered only the case where the magnetization vector $\mathbf{M} \parallel \hat{\mathbf{x}}$.

We have used the experimentally determined values for charge and magnetic resonant scattering amplitudes, $f_{c,m} = f'_{c,m} + if''_{c,m}$, at the resonant energy. The energy dependence of the absorption coefficient for opposite helicities, $\mu^\pm(E)$, were measured from a [Gd(51 Å)/Fe(34 Å)]₁₅ multilayer, which will be discussed below as an experimental example. The edge-step normalized $f''_{c,m}$ were obtained from the charge and magnetic absorption coefficients, $\mu_{c,m}$ [$\mu_c = (\mu^+ + \mu^-)/2$, $\mu_m = \mu^+ - \mu^-$], through the optical theorem, $f''_{c,m} \propto \mu_{c,m}$. Their absolute values were determined using the tabulated bare-atom scattering amplitudes away from resonance. Real parts were obtained from differential Kramers-Kronig transforms of imaginary parts. Figure 4(a) and (b) show the charge and magnetic scattering amplitudes around the Gd L₂-edge obtained in such absorption measurements. These values are in good agreement with the calculated ones from the listed values of A and B in Eq. (3.3) obtained from Ref. 8. For consistency of the definitions, it should be mentioned that the $f''_{c,m}$ used here correspond to $\text{Im}[A, B]$ in Eq. (3.3), whereas the $f'_{c,m}$ correspond to $-\text{Re}[A, B]$, respectively.

Figure 5 shows the calculated x-ray resonant magnetic reflectivities from a [Gd(51 Å)/Fe(34 Å)]₁₅ multilayer for different incident x-ray energies indicated in Fig. 4: (a) 7926 eV, (b) 7929 eV, (c) 7931 eV, and (d) 7935 eV. The lines and symbols represent the sum and difference in the reflected intensities for (+) and (−) circularly polarized incident x-rays, respectively, calculated using Eq. (7.5). Since the Gd/Fe multilayer was assumed to be sandwiched between Nb buffer (100 Å) and cap (30 Å) layers, the Kiessig fringes between the multilayer peaks in $(I_+ + I_-)$ intensities result from the interference of the scattering of Nb layers and thus show little energy dependence around the Gd absorption edge. On

the other hand, $(I_+ - I_-)$ intensities around the multilayer peaks show a clear energy dependence in signs and magnitudes relative to $(I_+ + I_-)$ intensities. In Fig. 5(a) and (d) at which energies f_m'' becomes much smaller than f_m' , the signs and relative magnitudes of $(I_+ - I_-)$ intensities follow simply the energy dependence of f_m' in Fig. 4(b), as expected in the kinematical approximation.¹⁹ At the energies close to the absorption edge where f_m'' cannot be neglected, however, one can hardly expect the signs and magnitudes of $(I_+ - I_-)$ intensities to be obtained directly from the values of f_m' and f_m'' in Fig. 4(b). Therefore, quantitative analysis on x-ray resonant magnetic reflectivity data at the resonant energy requires accurate calculation taking into account refraction and multiple scattering effects using dynamical theory, such as our self-consistent method presented above.

In order to study the effect of the magnetic roughness amplitude, $(I_+ - I_-)$ intensities for two cases, $\sigma_m < \sigma_c$ and $\sigma_m > \sigma_c$, have been calculated, as shown in Fig. 6. The calculations for $\sigma_m = \sigma_c$ have been shown in Fig. 5. For all cases, the charge roughness amplitudes were assumed to be $\sigma_{c,Fe/Gd} = 4.7 \text{ \AA}$ and $\sigma_{c,Gd/Fe} = 3.6 \text{ \AA}$. At the energy of 7935 eV, the intensities of $(I_+ - I_-)$ around the multilayer peaks are proportional to a simple Gaussian form, $\exp(-\sigma^2 q_z^2)$, as shown in Figs. 5(d), 6(a), and 6(b). This is consistent with the kinematical calculations,¹⁹ and σ for $(I_+ - I_-)$ corresponds to $\sqrt{(\sigma_c^2 + \sigma_m^2)/2}$ as given by the kinematical argument. On the other hand, at the energy of 7929 eV where f_m'' cannot be neglected, such a kinematical argument is no longer valid. Comparing Figs. 5(b), 6(c), and 6(d), we can see that the magnitudes of $(I_+ - I_-)$ peak intensities do not follow a Gaussian form, $\exp(-\sigma^2 q_z^2)$, but their signs change from negative (filled circles) to positive (open circles) values. This indicates that $(I_+ - I_-)$, which is known to be the charge-magnetic interference scattering in the kinematical theory,⁷ is sensitive even to the interference between charge and magnetic roughness amplitudes. However, it should be mentioned again that this result cannot be reproduced by the kinematical calculation but only by the dynamical one presented above.

Let us now consider the case where the magnetic structure in the resonant layers may not coincide with the chemical structure. For example, the ferromagnetic moments in Gd layers near Gd/Fe interfaces can be induced by the adjacent ferromagnetic Fe layers above the Curie temperature of Gd atoms,^{13,14} or a magnetically “dead layer” may exist at an interface between a ferromagnetic layer and an antiferromagnetic layer. Here we assume simply three different magnetization depth profiles in the Gd layers of a Gd/Fe multilayer,

as shown in Fig. 7: uniform magnetization (A), ferromagnetic moments only near the Gd/Fe interfaces (B), ferromagnetic moments near the centers of Gd layers between magnetically dead layers (C).

Figure 8 shows the results of calculations of x-ray resonant magnetic reflectivities from $[\text{Gd}(51 \text{ \AA})/\text{Fe}(34 \text{ \AA})]_{15}$ MLs with the different magnetic structures of Fig. 7. We assumed all magnetic roughness amplitudes of $\sigma_m = 4.2 \text{ \AA}$ (effectively same as σ_c) and the photon energy of $E = 7929 \text{ eV}$. In Figs. 8(a)-(c), Gd layers were assumed to be magnetized only near the Gd/Fe interfaces [model (B)], and the thickness of each magnetized layer was assumed to be 4.6 \AA (a), 8.4 \AA (b), and 12.8 \AA (c). On the other hand, in Fig. 8(d)-(f), Gd layers were assumed to be magnetized in the middle of each Gd layer and sandwiched between magnetically dead layers [model (C)], and the thickness of each dead layer was assumed to be 4.6 \AA (d), 8.4 \AA (e), and 12.8 \AA (f).

Unlike the case of uniform magnetization [model (A) in Fig. 7] shown in Fig. 5(b), $(I_+ - I_-)$ intensities in Fig. 8 for models (B) and (C) show no suppression in peak intensities due to the charge-magnetic interference, as discussed above. This may be ascribed to a spatial separation between the charge and magnetic interfaces in models (B) and (C), as shown in Fig. 7.

In addition, the signs and relative magnitudes of $(I_+ - I_-)$ intensities at the multilayer peaks change remarkably as the thicknesses of magnetized layers change. In general, the peak intensities of the $(m+n)$ -th order ML peak and its multiple orders are weak compared to other peak intensities when the thickness ratio between two constituent layers is n/m . For example, in our $\text{Gd}(51 \text{ \AA})/\text{Fe}(34 \text{ \AA})$ multilayer, the fifth peak corresponds to such a suppressed peak. Therefore, different thicknesses of magnetic layers readily change the order of the suppressed peak in $(I_+ - I_-)$ intensities, as shown in Fig. 8. On the other hand, the signs of $(I_+ - I_-)$ intensities for models (B) [Fig. 8(a)-(c)] and (C) [Fig. 8(d)-(f)] are opposite each other, because their magnetic structures are exactly reversed.

IX. EXPERIMENTS

X-ray resonant magnetic reflectivities were measured from an $\text{Fe}(34 \text{ \AA})/[\text{Gd}(51 \text{ \AA})/\text{Fe}(34 \text{ \AA})]_{15}$ multilayer. The multilayer was sputtered onto a Si substrate using Nb buffer (100 \AA) and cap (30 \AA) layers. SQUID magnetometry and XMCD measurements show that the

multilayer couples antiferromagnetically at the Gd/Fe interfaces and have coercive fields < 50 Oe at 300 K. X-ray measurements were performed at sector 4 of the Advanced Photon Source at Argonne National Laboratory. Undulator radiation was monochromatized with double Si(111) crystals and its polarization converted from linear to circular with a diamond (111) quarter-wave plate operated in Bragg transmission geometry.²⁹ The sample was placed in a $B = 2.1$ kG field parallel to its surface and in the scattering plane. Specular magnetic reflectivity was measured at room temperature with a photon energy near the Gd L_2 resonance (7929 eV) across multilayer Bragg peaks by switching the helicity of the incident radiation at each scattering vector $q_z = (4\pi/\lambda) \sin \theta$, with θ being the grazing incidence angle.

Figure 9 shows specular reflectivity curves obtained by adding [(a), $(I_+ + I_-)$] and subtracting [(b), $(I_+ - I_-)$] reflected intensities for opposite helicities of the incoming x-rays. Symbols represent measurements and solid lines represent the fits calculated using Eq. (7.5). From the fit for $(I_+ + I_-)$ intensities, we obtained the layer thicknesses $d_{\text{Gd}} = 50.74 \pm 0.09$ Å and $d_{\text{Fe}} = 33.98 \pm 0.09$ Å, and the roughness amplitudes of charge interfaces $\sigma_{c,\text{Fe/Gd}} = 4.7 \pm 0.1$ Å and $\sigma_{c,\text{Gd/Fe}} = 3.6 \pm 0.1$ Å. From the fit for $(I_+ - I_-)$ intensities, we found that the Gd layers were fully magnetized only near the Gd/Fe interfaces at room temperature, which is above the bulk T_c of Gd. This magnetization is induced by a strong antiferromagnetic exchange interaction with the magnetically ordered Fe layers.²⁷ From the best fit, the thickness of the ferromagnetic Gd layer was estimated to be 4.5 ± 0.3 Å, which is consistent with our previous work.¹⁴ Magnetic roughness amplitudes for Gd/Fe (Fe/Gd) and Gd-ferromagnetic/Gd-paramagnetic interfaces were estimated to be 4.2 ± 0.1 Å and 4.6 ± 0.1 Å, respectively.

X. CONCLUSIONS

The formulae for x-ray resonant magnetic specular reflectivity have been derived for both single and multiple interfaces using the self-consistent method in the framework of the distorted-wave Born approximation (DWBA). For this purpose, we have defined a structural and a magnetic interface to represent the actual interfaces. The well-known Nevot-Croce expression for the x-ray specular reflectivity from a rough surface has been generalized and examined for the case of a magnetically rough surface. The formalism has been generalized

to the case of multiple interfaces, as in the case of thin films or multilayers. Numerical illustrations have been given for typical examples of each of these systems and compared with the experimental data from a Gd/Fe multilayer. We have also presented the explicit expressions in the small-angle approximation, which are readily applicable to transition-metal and rare-earth L-edge resonant magnetic reflectivities. The code for the calculations in this paper is also available in C language by emailing to D.R.L. (drlee@aps.anl.gov).

Acknowledgments

Work at Argonne is supported by the U.S. DOE, Office of Basic Energy Sciences, under Contract No. W-31-109-Eng-38.

APPENDIX A: EXPLICIT EXPRESSIONS FOR $R_{\nu\mu}^{(0)}$, $T_{j\mu}^{(0)}$ USING 2×2 MATRIX FORMULAE

To calculate the explicit expressions for $R_{\nu\mu}^{(0)}$ and $T_{j\mu}^{(0)}$ in Eq. (4.4), we follow Stepanov and Sinha's approach¹⁵ developed for magnetic resonant reflections from ideally smooth interfaces. The electric field $\mathbf{E}_{z<0}(\mathbf{r})$ inside the magnetic medium with a dielectric susceptibility tensor given by Eq. (4.2) can be represented as

$$\mathbf{E}_{z<0}(\mathbf{r}) = \mathbf{E}e^{-ik_0uz+ik_0\cos\theta_ix}, \quad (\text{A1})$$

where θ_i is the incidence angle, as shown in Fig. 1. The parameter u can be a complex number due to absorption or total reflection. Substituting this in the wave equation Eq. (4.1), we obtain

$$\sum_{\beta} [(\sin^2\theta_i - u^2)\delta_{\alpha\beta} + n_{\alpha}n_{\beta} + \chi_{\alpha\beta}]E_{\beta} = 0, \quad (\text{A2})$$

where $n_{\alpha} = k_{\alpha}/k_0$, i.e., $n_x = \cos\theta_i$, $n_y = 0$, and $n_z = -u$.

If we consider the case where the magnetization vector is aligned along the sample surface in the scattering plane, i.e., $\mathbf{M} \parallel \hat{\mathbf{x}}$ in Fig. 1, the tensor $\chi_{\alpha\beta}$ of a resonant magnetic medium can be written from Eq. (3.5) as

$$(\chi_{\alpha\beta})_{\mathbf{M}\parallel\hat{\mathbf{x}}} = \left(\chi_1\delta_{\alpha\beta} - iB' \sum_{\gamma} \epsilon_{\alpha\beta\gamma} M_{\gamma} + C' M_{\alpha} M_{\beta} \right)_{\mathbf{M}\parallel\hat{\mathbf{x}}} = \begin{pmatrix} \chi_1 + C' & 0 & 0 \\ 0 & \chi_1 & -iB' \\ 0 & iB' & \chi_1 \end{pmatrix}, \quad (\text{A3})$$

where

$$\chi_1 = -\frac{4\pi}{k_0^2}\rho_0(\vec{r})r_0 + \frac{4\pi}{k_0^2}An_m(\vec{r}), \quad B' = \frac{4\pi}{k_0^2}Bn_m(\vec{r})M_x, \quad C' = \frac{4\pi}{k_0^2}Cn_m(\vec{r})M_x^2. \quad (\text{A4})$$

Assuming that the incidence angle θ_i is small ($\sin \theta_i \approx \theta_i \ll 1$ and $n_x = \cos \theta_i \approx 1$) and even at the resonance $\chi_{\alpha\beta}$ remain small ($|\chi_{\alpha\beta}| \ll 1$), and inserting Eq. (A3) into Eq. (A2), the dispersion equation for a nontrivial solution of Eq. (A2) can be then approximated by

$$\begin{vmatrix} 1 & 0 & -u \\ 0 & \theta_i^2 + \chi_1 - u^2 & -iB' \\ -u & iB' & \theta_i^2 + \chi_1 \end{vmatrix} = 0, \quad (\text{A5})$$

and the respective roots are $u^{(1,2,3,4)} = \pm\sqrt{\theta_i^2 + \chi_1 \pm B'}$. Two roots of these $u^{(j)}$'s with $\text{Im}[u^{(1,2)}] > 0$ and the other two roots with $\text{Im}[u^{(3,4)}] < 0$ correspond to transmitted and reflected waves in the medium, respectively. For each of the waves Eqs. (A2) and (A5) give ($j = 1, \dots, 4$)

$$E_z^{(j)} = \frac{\theta_i^2 + \chi_1 - u^{(j)2}}{iB'}E_y^{(j)}, \quad E_x^{(j)} = u^{(j)}\frac{\theta_i^2 + \chi_1 - u^{(j)2}}{iB'}E_y^{(j)}, \quad E_y^{(j)} = E_\sigma^{(j)}. \quad (\text{A6})$$

And if we denote

$$\begin{aligned} u^{(1)} &= \sqrt{\theta_i^2 + \chi_1 + B'} \equiv u_+, & u^{(2)} &= \sqrt{\theta_i^2 + \chi_1 - B'} \equiv u_-, \\ u^{(3)} &= -u_+, & u^{(4)} &= -u_-, \end{aligned} \quad (\text{A7})$$

we may then write

$$\begin{aligned} E_z^{(1)} &= iE_\sigma^{(1)}, & E_z^{(2)} &= -iE_\sigma^{(2)}, & E_z^{(3)} &= iE_\sigma^{(3)}, & E_z^{(4)} &= -iE_\sigma^{(4)}, \\ E_x^{(j)} &= u^{(j)}E_z^{(j)} \quad (j = 1, \dots, 4). \end{aligned} \quad (\text{A8})$$

Since $|u^{(j)}| \ll 1$, $E_x^{(j)}$ can be neglected, then the polarizations of the waves $\hat{\mathbf{e}}^{(j)}$ in the magnetic resonant medium can be reduced to the circular polarizations

$$\begin{aligned} \hat{\mathbf{e}}^{(j)} &\approx E_y^{(j)}\hat{\mathbf{e}}_\sigma + E_z^{(j)}\hat{\mathbf{e}}_\pi \quad (\hat{\mathbf{y}} = \hat{\mathbf{e}}_\sigma, \quad \hat{\mathbf{z}} \approx \hat{\mathbf{e}}_\pi), \\ \hat{\mathbf{e}}^{(1)} &= \hat{\mathbf{e}}_\sigma + i\hat{\mathbf{e}}_\pi = \hat{\mathbf{e}}^{(3)}, & \hat{\mathbf{e}}^{(2)} &= \hat{\mathbf{e}}_\sigma - i\hat{\mathbf{e}}_\pi = \hat{\mathbf{e}}^{(4)}. \end{aligned} \quad (\text{A9})$$

If the wave field $\mathbf{E}_{z>0}(\mathbf{r})$ with the incident and specularly reflected waves inside the non-magnetic(isotropic) medium can be represented as

$$\mathbf{E}_{z>0}(\mathbf{r}) = \left(\mathbf{E}_0 e^{-ik_0 u_0 z} + \mathbf{E}_R e^{ik_0 u_0 z} \right) e^{ik_0 \cos \theta_i x}, \quad \left(u_0 = \sqrt{\theta_i^2 + \chi_0} \right), \quad (\text{A10})$$

the boundary conditions for the waves, $\mathbf{E}_{z>0}(\mathbf{r})$ and $\mathbf{E}_{z<0}(\mathbf{r})$ in Eqs. (A1) and (A10) must be satisfied for the lateral components \mathbf{E}_{\parallel} and \mathbf{H}_{\parallel} of electric fields and magnetic fields, respectively. Since $\mathbf{H} \propto [\hat{\mathbf{k}} \times \mathbf{E}]$, this gives

$$\begin{aligned}
u_0 E_{0\pi} - u_0 E_{R\pi} &= \sum_j E_x^{(j)} \\
E_{0\sigma} + E_{R\sigma} &= \sum_j E_y^{(j)} \\
u_0 E_{0\sigma} - u_0 E_{R\sigma} &= u^{(j)} \sum_j E_y^{(j)} \\
E_{0\pi} + E_{R\pi} &= \sum_j (u^{(j)} E_x^{(j)} + n_x E_z^{(j)}) \approx \sum_j E_z^{(j)},
\end{aligned} \tag{A11}$$

where the approximation in the last equation was obtained by $|u^{(j)}| \ll 1$ and $n_x \approx 1$. Using Eqs. (A6)-(A8), the above equations can be expressed in the 4×4 matrix form

$$\begin{pmatrix} 1 & 0 & 1 & 0 \\ 0 & 1 & 0 & 1 \\ u_0 & 0 & -u_0 & 0 \\ 0 & u_0 & 0 & -u_0 \end{pmatrix} \begin{pmatrix} E_{0\sigma} \\ E_{0\pi} \\ E_{R\sigma} \\ E_{R\pi} \end{pmatrix} = \begin{pmatrix} 1 & 1 & 1 & 1 \\ i & -i & i & -i \\ u_+ & u_- & -u_+ & -u_- \\ iu_+ & -iu_- & -iu_+ & iu_- \end{pmatrix} \begin{pmatrix} E_{\sigma}^{(1)} \\ E_{\sigma}^{(2)} \\ E_{\sigma}^{(3)} \\ E_{\sigma}^{(4)} \end{pmatrix}. \tag{A12}$$

Representing the waves as the vectors $T_0 = (E_{0\sigma}, E_{0\pi})$, $R_0 = (E_{R\sigma}, E_{R\pi})$, $T_1 = (E_{\sigma}^{(1)}, E_{\sigma}^{(2)})$, and $R_1 = (E_{\sigma}^{(3)}, E_{\sigma}^{(4)})$, the 4×4 matrices in Eq. (A12) can be reduced into four 2×2 blocks

$$\begin{pmatrix} T_0 \\ R_0 \end{pmatrix} = \begin{pmatrix} X^{tt} & X^{tr} \\ X^{rt} & X^{rr} \end{pmatrix} \begin{pmatrix} T_1 \\ R_1 \end{pmatrix}, \tag{A13}$$

where X^{tt} , X^{tr} , X^{rt} , X^{rr} can be obtained by multiplying the inverse of the 4×4 matrix at the left side of Eq. (A12) onto the both sides. Since the reflected waves inside the medium vanish for a single surface, $\mathbf{E}^{(3)} = \mathbf{E}^{(4)} = 0$ [i.e., $R_1 = (0, 0)$], the ‘‘unknown’’ waves R_0 and T_1 in Eq. (A13) can be expressed via the ‘‘known’’ waves T_0 and R_1 as

$$\begin{pmatrix} T_1 \\ R_0 \end{pmatrix} = \begin{pmatrix} M^{tt} & M^{tr} \\ M^{rt} & M^{rr} \end{pmatrix} \begin{pmatrix} T_0 \\ R_1 \end{pmatrix}, \tag{A14}$$

where

$$\begin{aligned}
M^{tt} &= (X^{tt})^{-1}, \quad M^{tr} = -(X^{tt})^{-1} X^{tr}, \\
M^{rt} &= X^{rt} (X^{tt})^{-1}, \quad M^{rr} = X^{rr} - X^{rt} (X^{tt})^{-1} X^{tr}.
\end{aligned} \tag{A15}$$

From Eqs. (A12)-(A15), the explicit expressions for $M_{n \rightarrow r}^{pq}$ matrices are given by

$$\begin{aligned}
M_{n \rightarrow r}^{tt} &= \begin{pmatrix} \frac{u_0}{u_0+u_+} & -i \frac{u_0}{u_0+u_+} \\ \frac{u_0}{u_0+u_-} & i \frac{u_0}{u_0+u_-} \end{pmatrix} = T_{j\mu}^{(0)}(\mathbf{k}_i), \\
M_{n \rightarrow r}^{tr} &= \begin{pmatrix} \frac{u_+-u_0}{u_0+u_+} & 0 \\ 0 & \frac{u_- - u_0}{u_0+u_-} \end{pmatrix}, \\
M_{n \rightarrow r}^{rt} &= \begin{pmatrix} \frac{u_0^2 - u_+ u_-}{(u_0+u_+)(u_0+u_-)} & i \frac{u_0(u_+-u_-)}{(u_0+u_+)(u_0+u_-)} \\ -i \frac{u_0(u_+-u_-)}{(u_0+u_+)(u_0+u_-)} & \frac{u_0^2 - u_+ u_-}{(u_0+u_+)(u_0+u_-)} \end{pmatrix} = R_{\nu\mu}^{(0)}(\mathbf{k}_i), \\
M_{n \rightarrow r}^{rr} &= \begin{pmatrix} \frac{2u_+}{u_0+u_+} & \frac{2u_-}{u_0+u_-} \\ i \frac{2u_+}{u_0+u_+} & -i \frac{2u_-}{u_0+u_-} \end{pmatrix}, \tag{A16}
\end{aligned}$$

where the ij -elements of M^{pq} matrices are defined by Fig. 10, and the subscript $n \rightarrow r$ represents the incidence from a nonmagnetic medium into a resonant magnetic one. From the definition of M^{pq} matrices in Eq. (A14), $R_{\nu\mu}^{(0)}(\mathbf{k}_i)$ and $T_{j\mu}^{(0)}(\mathbf{k}_i)$ correspond to $M_{n \rightarrow r}^{rt}$ and $M_{n \rightarrow r}^{tt}$, respectively. For the time-reversed waves incident with vector $(-\mathbf{k}_f)$, scattering angle θ_f , and polarization ν , $M_{n \rightarrow r}^{pq}(-\mathbf{k}_f)$ matrices are same as the case of (\mathbf{k}_i, μ) but replacing i by $(-i)$ in Eq. (A16), i.e.,

$$\begin{aligned}
M_{n \rightarrow r}^{pq}(-\mathbf{k}_f) &= M_{n \rightarrow r}^{pq}(\mathbf{k}_i; i \leftrightarrow -i), \quad (pq = tt, tr, rt, rr), \\
T_{j\mu}^{(0)}(-\mathbf{k}_f) &= T_{j\mu}^{(0)}(\mathbf{k}_i; i \leftrightarrow -i), \quad R_{\nu\mu}^{(0)}(-\mathbf{k}_f) = R_{\nu\mu}^{(0)}(\mathbf{k}_i; i \leftrightarrow -i). \tag{A17}
\end{aligned}$$

For completeness, let us now consider the reverse case where a wave is incident ‘‘from’’ a magnetic (anisotropic) medium with $\chi_{\alpha\beta} = \chi_1 \delta_{\alpha\beta} + \chi_{\alpha\beta}^{(2)}$ ‘‘into’’ a nonmagnetic one with $\chi_{\alpha\beta} = \chi_0 \delta_{\alpha\beta}$. The explicit forms of $M_{r \rightarrow n}^{pq}$ matrices can be evaluated by starting with reversing both sides in Eq. (A12) and representing the waves as $T_0 = (E_\sigma^{(1)}, E_\sigma^{(2)})$, $R_0 = (E_\sigma^{(3)}, E_\sigma^{(4)})$, $T_1 = (E_{0\sigma}, E_{0\pi})$, and $R_1 = (E_{R\sigma}, E_{R\pi})$ in Eq. (A13). Then, $M_{r \rightarrow n}^{pq}$ matrices can be obtained straightforwardly by

$$\begin{aligned}
M_{r \rightarrow n}^{tt} &= T_{\mu j}^{(0)}(\mathbf{k}_i) = M_{n \rightarrow r}^{rr}, \quad M_{r \rightarrow n}^{tr} = M_{n \rightarrow r}^{rt}, \\
M_{r \rightarrow n}^{rt} &= R_{j j'}^{(0)}(\mathbf{k}_i) = M_{n \rightarrow r}^{tr}, \quad M_{r \rightarrow n}^{rr} = M_{n \rightarrow r}^{tt}, \tag{A18}
\end{aligned}$$

where the subscript $r \rightarrow n$ denotes the incidence from a resonant magnetic medium into a nonmagnetic one. In the same way as in Eq. (A17), the $M_{r \rightarrow n}^{pq}(-\mathbf{k}_f)$ matrices for the time-reversed waves can be also obtained by replacing i by $(-i)$ in Eq. (A18).

Finally, let us also consider the magnetic-magnetic (resonant-resonant) interface between upper ($\chi_{\alpha\beta,\text{up}} = \chi_{\text{up}}\delta_{\alpha\beta} + \chi_{\alpha\beta,\text{up}}^{(2)}$) and lower ($\chi_{\alpha\beta,\text{dw}} = \chi_{\text{dw}}\delta_{\alpha\beta} + \chi_{\alpha\beta,\text{dw}}^{(2)}$) resonant magnetic layers. By employing the 4×4 matrices involving resonant magnetic medium to both sides of Eq. (A12), the explicit expressions of $M_{r \rightarrow r}^{pq}$ can be given by

$$\begin{aligned}
M_{r \rightarrow r}^{tt} &= \begin{pmatrix} \frac{2u_+^{\text{up}}}{u_+^{\text{dw}} + u_+^{\text{up}}} & 0 \\ 0 & \frac{2u_-^{\text{up}}}{u_-^{\text{dw}} + u_-^{\text{up}}} \end{pmatrix}, \\
M_{r \rightarrow r}^{tr} &= \begin{pmatrix} \frac{u_+^{\text{dw}} - u_+^{\text{up}}}{u_+^{\text{dw}} + u_+^{\text{up}}} & 0 \\ 0 & \frac{u_-^{\text{dw}} - u_-^{\text{up}}}{u_-^{\text{dw}} + u_-^{\text{up}}} \end{pmatrix}, \quad M_{r \rightarrow r}^{rt} = -M_{r \rightarrow r}^{tr} \\
M_{r \rightarrow r}^{rr} &= \begin{pmatrix} \frac{2u_+^{\text{dw}}}{u_+^{\text{dw}} + u_+^{\text{up}}} & 0 \\ 0 & \frac{2u_-^{\text{dw}}}{u_-^{\text{dw}} + u_-^{\text{up}}} \end{pmatrix}, \tag{A19}
\end{aligned}$$

where $u_{\pm}^{\text{up,dw}} = \sqrt{\theta_i^2 + \chi_{\text{up,dw}} \pm B'_{\text{up,dw}}}$ and $B'_{\text{up,dw}}$ was defined in Eq. (A4). Note that these $M_{r \rightarrow r}^{pq}$ matrices for the magnetic-magnetic interfaces are applicable to the nonmagnetic-nonmagnetic (nonresonant-nonresonant) interfaces simply by setting $B'_{\text{up,dw}}$ to be zero.

APPENDIX B: EVALUATION OF THE MATRIX ELEMENTS INVOLVING $\chi^{(0)}$

To evaluate the matrix element in Eqs. (4.15) and (5.12), we assume that $\chi_0 = 0$ in Eq. (4.7), i.e., the first nonmagnetic medium is vacuum. Then the matrix element in Eq. (4.15) can be evaluated from Eqs. (4.3) and (4.10) as

$$\begin{aligned}
k_0^2 \langle -\mathbf{k}_f^T, \nu | \boldsymbol{\chi}^{(0)} | \mathbf{E}_{\mu}^i(\mathbf{r}) \rangle &= \mathcal{A}k_0^2 \delta_{k_{ix}k_{fx}} \delta_{k_{iy}k_{fy}} \sum_j T_{j\nu}^{(0)}(-\mathbf{k}_f) \\
&\times \sum_{\alpha\beta} e_{j\alpha}^* (\chi_1 \delta_{\alpha\beta} + \chi_{\alpha\beta}^{(2)}) e_{\mu\beta} \int_{-\infty}^0 dz e^{-i(k_{fz}^t(j) - k_{iz})z}, \\
&= i\mathcal{A}k_0^2 \delta_{k_{ix}k_{fx}} \delta_{k_{iy}k_{fy}} \\
&\times \sum_j \frac{T_{j\nu}^{(0)}(-\mathbf{k}_f)}{k_{fz}^t(j) - k_{iz}} \sum_{\alpha\beta} e_{j\alpha}^* (\chi_1 \delta_{\alpha\beta} + \chi_{\alpha\beta}^{(2)}) e_{\mu\beta}. \tag{B1}
\end{aligned}$$

In order to evaluate the explicit expression for the above equation, let us now consider the case where the incidence angle θ_i is small and $\mathbf{M} \parallel \hat{\mathbf{x}}$, as discussed in Appendix A. In this case, $\hat{\mathbf{e}}_j = \hat{\mathbf{e}}_{\sigma} \pm i\hat{\mathbf{e}}_{\pi}$ and $k_{fz}^t(j) = k_0 u_{\pm}$, where the upper and lower signs correspond to $j = 1$ and 2 , respectively, and $k_{iz} = -k_0 u_0$. From Eqs. (4.2), (A4), and (A7), the

polarization-dependent terms are evaluated by

$$\begin{aligned} \sum_{\alpha\beta} e_{j\alpha}^* (\chi_1 \delta_{\alpha\beta} + \chi_{\alpha\beta}^{(2)}) e_{\mu\beta} &= \chi_1 (\hat{\mathbf{e}}_j^* \cdot \hat{\mathbf{e}}_\mu) + (\hat{\mathbf{e}}_j^* \times \hat{\mathbf{e}}_\mu)_x \chi_{\mathbf{M} \parallel \hat{\mathbf{x}}}^{(2)} \\ &= \begin{cases} \chi_1 + i\chi^{(2)} = u_+^2 - u_0^2, & \text{for } j = 1, \mu = \sigma \\ \chi_1 - i\chi^{(2)} = u_-^2 - u_0^2, & \text{for } j = 2, \mu = \sigma \\ -i\chi_1 + \chi^{(2)} = -i(u_+^2 - u_0^2), & \text{for } j = 1, \mu = \pi \\ i\chi_1 + \chi^{(2)} = i(u_-^2 - u_0^2), & \text{for } j = 2, \mu = \pi \end{cases}, \quad (\text{B2}) \end{aligned}$$

where $u_0 = \theta_i$ when $\chi_0 = 0$ in Eq. (A10). The explicit form of 2×2 matrix $T_{j\nu}^{(0)}(-\mathbf{k}_f)$ can be obtained from $M_{n \rightarrow r}^{tt}$ in Eq. (A16) by replacing i by $(-i)$. Then, the matrix element in Eq. (4.15) can be expressed by 2×2 matrix in terms of the polarizations of incident and outgoing beams, μ and ν , as follows:

$$\begin{aligned} k_0^2 \langle -\mathbf{k}_f^T, \nu | \chi^{(0)} | \mathbf{E}_\mu^i(\mathbf{r}) \rangle &= i\mathcal{A}k_0^2 \delta_{k_{ix}k_{fx}} \delta_{k_{iy}k_{fy}} \frac{2u_0}{k_0(u_+ + u_0)(u_- + u_0)} \\ &\times \begin{pmatrix} u_+u_- - u_0^2 & -iu_0(u_+ - u_-) \\ iu_0(u_+ - u_-) & u_+u_- - u_0^2 \end{pmatrix}, \\ &= 2i\mathcal{A}k_{iz}R_{\nu\mu}^{(0)}(\mathbf{k}_i) \delta_{k_{ix}k_{fx}} \delta_{k_{iy}k_{fy}}, \quad (\text{B3}) \end{aligned}$$

where $R_{\nu\mu}^{(0)}(\mathbf{k}_i)$ corresponds to $M_{n \rightarrow r}^{rt}$ in Eq. (A16). Without loss of generality the final result in Eq. (B3) is applicable for the case with $\chi_0 \neq 0$ although the calculation for $z > 0$ should be included in Eqs. (B1)-(B3).

For the transmission coefficient, the matrix element in Eq. (5.12) for $\chi_0 = 0$ can be also evaluated from Eqs. (5.10) and (5.11) as

$$\begin{aligned} k_0^2 \langle -\mathbf{k}_f^T, j | \chi^{(0)} | \mathbf{k}_i, \mu \rangle &= \mathcal{A}k_0^2 \delta_{k_{ix}k_{fx}} \delta_{k_{iy}k_{fy}} \sum_\nu T_{\nu j}^{(0)}(-\mathbf{k}_f) \sum_{j'} T_{j'\mu}^{(0)}(\mathbf{k}_i) \\ &\times \sum_{\alpha\beta} e_{\nu\alpha}^* (\chi_1 \delta_{\alpha\beta} + \chi_{\alpha\beta}^{(2)}) e_{j'\beta} \int_{-\infty}^0 dz e^{-i(-k_{fz} - k_{iz}^t(j'))z}, \\ &= i\mathcal{A}k_0^2 \delta_{k_{ix}k_{fx}} \delta_{k_{iy}k_{fy}} \\ &\times \sum_{\nu, j'} \frac{T_{\nu j}^{(0)}(-\mathbf{k}_f) T_{j'\mu}^{(0)}(\mathbf{k}_i)}{-k_{fz} - k_{iz}^t(j')} \sum_{\alpha\beta} e_{\nu\alpha}^* (\chi_1 \delta_{\alpha\beta} + \chi_{\alpha\beta}^{(2)}) e_{j'\beta}, \quad (\text{B4}) \end{aligned}$$

where the vector field $\mathbf{E}(\mathbf{k}_i, \mu)$ in Eq. (5.10) has been used for the state $|\mathbf{k}_i, \mu\rangle$ instead of the ‘‘pure’’ incoming wave $\mathbf{E}_\mu^i(\mathbf{r})$ in Eq. (4.3). Similarly to the reflection coefficient in Eqs. (B1)-(B3), the matrix element in Eq. (5.12) can be expressed by a 2×2 matrix in terms of

the polarizations of incident and transmitted beams, μ and j , as follows:

$$\begin{aligned}
k_0^2 \langle -\mathbf{k}_f^T, j | \chi^{(0)} | \mathbf{k}_i, \mu \rangle &= i \mathcal{A} k_0^2 \delta_{k_{ix} k_{fx}} \delta_{k_{iy} k_{fy}} \frac{4}{k_0} \begin{pmatrix} u_+ \frac{u_0}{u_+ + u_0} & u_+ \frac{-iu_0}{u_+ + u_0} \\ u_- \frac{u_0}{u_- + u_0} & u_- \frac{iu_0}{u_- + u_0} \end{pmatrix}, \\
&= 4i \mathcal{A} k_{iz}^t(j) \delta_{k_{ix} k_{fx}} \delta_{k_{iy} k_{fy}} \begin{pmatrix} \frac{u_0}{u_+ + u_0} & \frac{-iu_0}{u_+ + u_0} \\ \frac{u_0}{u_- + u_0} & \frac{iu_0}{u_- + u_0} \end{pmatrix}, \\
&= 4i \mathcal{A} k_{iz}^t(j) T_{j\mu}^{(0)}(\mathbf{k}_i) \delta_{k_{ix} k_{fx}} \delta_{k_{iy} k_{fy}}, \tag{B5}
\end{aligned}$$

where $T_{j\mu}^{(0)}(\mathbf{k}_i)$ corresponds to $M_{n \rightarrow r}^{tt}$ in Eq. (A16). Again, the final result in Eq. (B5) is applicable for the case with $\chi_0 \neq 0$ without loss of generality.

APPENDIX C: EXPLICIT EXPRESSIONS FOR ROUGH-INTERFACE \tilde{M}^{pq} MATRICES

For the interface between upper nonmagnetic ($\chi_{\alpha\beta} = \chi_0 \delta_{\alpha\beta}$) and lower resonant magnetic ($\chi_{\alpha\beta} = \chi_1 \delta_{\alpha\beta} + \chi_{\alpha\beta}^{(2)}$) layers, the explicit expressions of the rough-interface $\tilde{M}_{n \rightarrow r}^{pq}$ matrices can be given by

$$\begin{aligned}
\tilde{M}_{n \rightarrow r}^{rt} &= \mathbf{R}_{n \rightarrow r} = (\mathbf{I} - \mathbf{V}_{n \rightarrow r})^{-1} (\mathbf{R}_{n \rightarrow r}^{(0)} + \mathbf{U}_{n \rightarrow r}), \\
\tilde{M}_{n \rightarrow r}^{tt} &= \mathbf{T}_{n \rightarrow r} = (\mathbf{I} - \mathbf{V}'_{n \rightarrow r})^{-1} \mathbf{T}_{n \rightarrow r}^{(0)}, \tag{C1}
\end{aligned}$$

where, from Eqs. (5.6) and (5.19),

$$\begin{aligned}
\mathbf{R}_{n \rightarrow r}^{(0)} + \mathbf{U}_{n \rightarrow r} &= -\frac{1}{2} \begin{pmatrix} \frac{D_1^{(+)} + D_2^{(+)}}{(u_+ + u_0)^2} + \frac{D_3^{(+)} - D_4^{(+)}}{(u_- + u_0)^2} & -i \left(\frac{D_1^{(+)} + D_2^{(+)}}{(u_+ + u_0)^2} - \frac{D_3^{(+)} - D_4^{(+)}}{(u_- + u_0)^2} \right) \\ i \left(\frac{D_1^{(+)} + D_2^{(+)}}{(u_+ + u_0)^2} - \frac{D_3^{(+)} - D_4^{(+)}}{(u_- + u_0)^2} \right) & \frac{D_1^{(+)} + D_2^{(+)}}{(u_+ + u_0)^2} + \frac{D_3^{(+)} - D_4^{(+)}}{(u_- + u_0)^2} \end{pmatrix}, \\
\mathbf{I} - \mathbf{V}_{n \rightarrow r} &= \frac{1}{2} \begin{pmatrix} \frac{D_1^{(-)} + D_2^{(-)}}{u_+^2 - u_0^2} + \frac{D_3^{(-)} - D_4^{(-)}}{u_-^2 - u_0^2} & -i \left(\frac{D_1^{(-)} + D_2^{(-)}}{u_+^2 - u_0^2} - \frac{D_3^{(-)} - D_4^{(-)}}{u_-^2 - u_0^2} \right) \\ i \left(\frac{D_1^{(-)} + D_2^{(-)}}{u_+^2 - u_0^2} - \frac{D_3^{(-)} - D_4^{(-)}}{u_-^2 - u_0^2} \right) & \frac{D_1^{(-)} + D_2^{(-)}}{u_+^2 + u_0^2} + \frac{D_3^{(-)} - D_4^{(-)}}{u_-^2 - u_0^2} \end{pmatrix}, \\
\mathbf{I} - \mathbf{V}'_{n \rightarrow r} &= \begin{pmatrix} \frac{D_1^{(-)} + D_2^{(-)}}{u_+^2 - u_0^2} & 0 \\ 0 & \frac{D_3^{(-)} - D_4^{(-)}}{u_-^2 - u_0^2} \end{pmatrix}, \\
\mathbf{T}_{n \rightarrow r}^{(0)} = M_{n \rightarrow r}^{tt} &= \begin{pmatrix} \frac{u_0}{u_+ + u_0} & -i \frac{u_0}{u_+ + u_0} \\ \frac{u_0}{u_- + u_0} & i \frac{u_0}{u_- + u_0} \end{pmatrix}, \tag{C2}
\end{aligned}$$

and

$$\begin{aligned}
D_1^{(\pm)} &= (\chi_1 - \chi_0) e^{-\frac{k_0^2}{2}(u_+ \pm u_0)^2 \sigma_c^2}, \quad D_2^{(\pm)} = B' e^{-\frac{k_0^2}{2}(u_+ \pm u_0)^2 \sigma_m^2}, \\
D_3^{(\pm)} &= (\chi_1 - \chi_0) e^{-\frac{k_0^2}{2}(u_- \pm u_0)^2 \sigma_c^2}, \quad D_4^{(\pm)} = B' e^{-\frac{k_0^2}{2}(u_- \pm u_0)^2 \sigma_m^2}. \tag{C3}
\end{aligned}$$

Here, $(\chi_1 - \chi_0) = (u_+^2 + u_-^2)/2 - u_0^2$ and $B' = (u_+^2 - u_-^2)/2$ can be used from $u_0 = \sqrt{\theta_i^2 + \chi_0}$ and $u_{\pm} = \sqrt{\theta_i^2 + \chi_1 \pm B'}$.

For the reversed interface between upper magnetic(resonant) and lower nonmagnetic layers, $\tilde{M}_{r \rightarrow n}^{pq}$ matrices can be also given by

$$\begin{aligned}\tilde{M}_{r \rightarrow n}^{rt} &= \mathbf{R}_{r \rightarrow n} = (\mathbf{I} - \mathbf{V}_{r \rightarrow n})^{-1}(\mathbf{R}_{r \rightarrow n}^{(0)} + \mathbf{U}_{r \rightarrow n}), \\ \tilde{M}_{r \rightarrow n}^{tt} &= \mathbf{T}_{r \rightarrow n} = (\mathbf{I} - \mathbf{V}'_{r \rightarrow n})^{-1}\mathbf{T}_{r \rightarrow n}^{(0)},\end{aligned}\quad (\text{C4})$$

where

$$\begin{aligned}\mathbf{R}_{r \rightarrow n}^{(0)} + \mathbf{U}_{r \rightarrow n} &= \begin{pmatrix} \frac{D_1^{(+)} + D_2^{(+)}}{(u_+ + u_0)^2} & 0 \\ 0 & \frac{D_3^{(+)} - D_4^{(+)}}{(u_- + u_0)^2} \end{pmatrix}, \\ \mathbf{I} - \mathbf{V}_{r \rightarrow n} &= \mathbf{I} - \mathbf{V}'_{n \rightarrow r}, \quad \mathbf{I} - \mathbf{V}'_{r \rightarrow n} = \mathbf{I} - \mathbf{V}_{n \rightarrow r}, \\ \mathbf{T}_{r \rightarrow n}^{(0)} &= M_{r \rightarrow n}^{tt} = \begin{pmatrix} \frac{2u_+}{u_+ + u_0} & \frac{2u_-}{u_- + u_0} \\ i\frac{2u_+}{u_+ + u_0} & -i\frac{2u_-}{u_- + u_0} \end{pmatrix}.\end{aligned}\quad (\text{C5})$$

In the same way as Eq. (A18), other \tilde{M}^{pq} matrices can be given by

$$\tilde{M}_{n \rightarrow r}^{tr} = \tilde{M}_{r \rightarrow n}^{rt}, \quad \tilde{M}_{n \rightarrow r}^{rr} = \tilde{M}_{r \rightarrow n}^{tt}, \quad \tilde{M}_{r \rightarrow n}^{tr} = \tilde{M}_{n \rightarrow r}^{rt}, \quad \tilde{M}_{r \rightarrow n}^{rr} = \tilde{M}_{n \rightarrow r}^{tt}.\quad (\text{C6})$$

Finally, for the magnetic-magnetic (resonant-resonant) interface between upper resonant magnetic ($\chi_{\alpha\beta}^{\text{up}} = \chi_1^{\text{up}}\delta_{\alpha\beta} + \chi_{\alpha\beta}^{(2),\text{up}}$) and lower resonant magnetic ($\chi_{\alpha\beta}^{\text{dw}} = \chi_1^{\text{dw}}\delta_{\alpha\beta} + \chi_{\alpha\beta}^{(2),\text{dw}}$) layers, $\tilde{M}_{r \rightarrow n}^{pq}$ matrices can be also given by

$$\begin{aligned}\tilde{M}_{r \rightarrow r}^{rt} &= \mathbf{R}_{r \rightarrow r} = (\mathbf{I} - \mathbf{V}_{r \rightarrow r})^{-1}(\mathbf{R}_{r \rightarrow r}^{(0)} + \mathbf{U}_{r \rightarrow r}), \\ \tilde{M}_{r \rightarrow r}^{tt} &= \mathbf{T}_{r \rightarrow r} = (\mathbf{I} - \mathbf{V}'_{r \rightarrow r})^{-1}\mathbf{T}_{r \rightarrow r}^{(0)},\end{aligned}\quad (\text{C7})$$

where

$$\begin{aligned}\mathbf{R}_{r \rightarrow r}^{(0)} + \mathbf{U}_{r \rightarrow r} &= - \begin{pmatrix} \frac{D_5^{(+)} + D_6^{(+)}}{(u_+^{\text{dw}} + u_+^{\text{up}})^2} & 0 \\ 0 & \frac{D_7^{(+)} - D_8^{(+)}}{(u_-^{\text{dw}} + u_-^{\text{up}})^2} \end{pmatrix}, \\ \mathbf{I} - \mathbf{V}_{r \rightarrow r} &= \begin{pmatrix} \frac{D_5^{(-)} + D_6^{(-)}}{(u_+^{\text{dw}})^2 - (u_+^{\text{up}})^2} & 0 \\ 0 & \frac{D_7^{(-)} - D_8^{(-)}}{(u_-^{\text{dw}})^2 - (u_-^{\text{up}})^2} \end{pmatrix},\end{aligned}\quad (\text{C8})$$

and

$$\begin{aligned}D_5^{(\pm)} &= (\chi_1^{\text{dw}} - \chi_1^{\text{up}})e^{-\frac{k_0^2}{2}(u_+^{\text{dw}} \pm u_+^{\text{up}})^2\sigma_c^2}, \quad D_6^{(\pm)} = (B'_{\text{dw}} - B'_{\text{up}})e^{-\frac{k_0^2}{2}(u_+^{\text{dw}} \pm u_+^{\text{up}})^2\sigma_m^2}, \\ D_7^{(\pm)} &= (\chi_1^{\text{dw}} - \chi_1^{\text{up}})e^{-\frac{k_0^2}{2}(u_-^{\text{dw}} \pm u_-^{\text{up}})^2\sigma_c^2}, \quad D_8^{(\pm)} = (B'_{\text{dw}} - B'_{\text{up}})e^{-\frac{k_0^2}{2}(u_-^{\text{dw}} \pm u_-^{\text{up}})^2\sigma_m^2},\end{aligned}\quad (\text{C9})$$

and $(\mathbf{I} - \mathbf{V}'_{r \rightarrow r})$ corresponds to $(\mathbf{I} - \mathbf{V}_{r \rightarrow r})$ when switching the upper and lower layers, and $\mathbf{T}_{r \rightarrow r}^{(0)}$ corresponds to $M_{r \rightarrow r}^{tt}$ in Eq. (A19). Here, $(\chi_1^{\text{dw}} - \chi_1^{\text{up}}) = [(u_+^{\text{dw}})^2 + (u_-^{\text{dw}})^2]/2 - [(u_+^{\text{up}})^2 + (u_-^{\text{up}})^2]/2$ and $(B'_{\text{dw}} - B'_{\text{up}}) = [(u_+^{\text{dw}})^2 - (u_-^{\text{dw}})^2]/2 - [(u_+^{\text{up}})^2 - (u_-^{\text{up}})^2]/2$ can be used from $u_{\pm}^{\text{up,dw}} = \sqrt{\theta_i^2 + \chi_1^{\text{up,dw}} \pm B'_{\text{up,dw}}}$. In the same way as Eq. (C6), two other matrices $\tilde{M}_{r \rightarrow r}^{tr}$ and $\tilde{M}_{r \rightarrow r}^{rr}$ can be also obtained from $\tilde{M}_{r \rightarrow r}^{rt}$ and $\tilde{M}_{r \rightarrow r}^{tt}$ in Eq. (C7), respectively, by switching the upper and lower layers. We should mention again that these rough-interface \tilde{M}^{pq} matrices for the magnetic-magnetic (resonant-resonant) interfaces can be reduced to the cases for the nonmagnetic-nonmagnetic (nonresonant-nonresonant) interfaces by setting $B'_{\text{up,dw}}$ to be zero.

APPENDIX D: SOLUTIONS OF SELF-CONSISTENT MATRIX EQUATIONS FOR NONMAGNETIC INTERFACES

For nonmagnetic interfaces ($|\mathbf{M}| = 0$) and $\sigma \rightarrow \sigma$ polarization, simply

$$u_+ = u_- = \sqrt{\theta_i^2 + \chi_1} = |k_z^t|/k_0. \quad (\text{D1})$$

Inserting this in Eq. (A16) modified for $(-\mathbf{k}_f)$ and using $\chi_1 - \chi_0 = (|k_z^t|^2 - |k_z|^2)/k_0^2$, the self-consistent solution for the reflection coefficient ($\mathbf{k}_f = \mathbf{k}_i^r$ and $\theta_i = \theta_f$) in Eq. (5.6) can be reduced to a scalar as

$$R = (1 - V)^{-1}(R^{(0)} + U), \quad (\text{D2})$$

where

$$\begin{aligned} U &= \frac{|k_z| - |k_z^t|}{|k_z| + |k_z^t|} \left(e^{-\frac{1}{2}(|k_z| + |k_z^t|)^2 \sigma_c^2} - 1 \right), \\ R^{(0)} &= \frac{|k_z| - |k_z^t|}{|k_z| + |k_z^t|}, \\ V &= 1 - e^{-\frac{1}{2}(|k_z| - |k_z^t|)^2 \sigma_c^2}, \end{aligned} \quad (\text{D3})$$

and $k_{fz}^t = |k_z^t|$, and $k_{iz} = -k_{iz}^r = -|k_z|$. Then, we obtain

$$R = \frac{|k_z| - |k_z^t|}{|k_z| + |k_z^t|} e^{-\frac{1}{2}(|k_z| + |k_z^t|)^2 \sigma_c^2} e^{+\frac{1}{2}(|k_z| - |k_z^t|)^2 \sigma_c^2} = R^{(0)} e^{-2|k_z||k_z^t| \sigma_c^2}, \quad (\text{D4})$$

which is consistent with the Nevot-Croce form.²¹

Similarly, the self-consistent solution for the transmission coefficient in Eq. (5.19) can be reduced into a scalar as

$$T_{(\sigma\sigma)} = \sum_{j=1,2} T_{j\sigma} = \sum_{j=1,2} (1 - V')^{-1} T_{j\sigma}^{(0)}, \quad (\text{D5})$$

where

$$\begin{aligned} V' &= 1 - e^{-\frac{1}{2}(|k_z| - |k_z^t|)^2 \sigma_c^2}, \\ T_{1\sigma}^{(0)} &= T_{2\sigma}^{(0)} = \frac{|k_z|}{|k_z| + |k_z^t|}. \end{aligned} \quad (\text{D6})$$

Then,

$$T = \frac{2|k_z|}{|k_z| + |k_z^t|} e^{\frac{1}{2}(|k_z| - |k_z^t|)^2 \sigma_c^2} = T^{(0)} e^{\frac{1}{2}(|k_z| - |k_z^t|)^2 \sigma_c^2}, \quad (\text{D7})$$

which is consistent with the Vidal-Vincent form.²³

APPENDIX E: RECURSIVE 2×2 MATRIX FORMULAE FOR MULTIPLE INTERFACES

For multiple interfaces, additional phase differences between different interfaces should be taken into account to extend the results for a single interface in Appendix A. Following Ref. 15, M_{n+1}^{pq} matrices for the n -th interface between n - and $(n+1)$ -th layers can be modified from Eq. (A15) as

$$M_{n+1}^{tt} = M^{tt} F_n^{-1}, \quad M_{n+1}^{tr} = M^{tr}, \quad M_{n+1}^{rt} = F_n^{-1} M^{rt} F_n^{-1}, \quad M_{n+1}^{rr} = F_n^{-1} M^{rr}, \quad (\text{E1})$$

where M^{pq} are the 2×2 matrices obtained for a single smooth interface in Appendix A, depending on whether the upper and lower layers on the n -th interface are nonmagnetic or magnetic ones, respectively,

$$F_n = \begin{pmatrix} e^{-ik_0 u_{+,n} d_n} & 0 \\ 0 & e^{-ik_0 u_{-,n} d_n} \end{pmatrix}, \quad (\text{E2})$$

and $u_{\pm,n}$ and d_n represent the refracted angle defined in Eq. (A7) and the thickness of the n -th (upper) layer, respectively. For nonmagnetic layers, $u_{\pm,n}$ reduces to $u_{0,n}$ in Eq. (A10). R_n and T_n are the vectors $(R_{n,1}, R_{n,2})$ and $(T_{n,1}, T_{n,2})$ representing the two waves reflected and transmitted, respectively, at the top of the n -th layer. (In Ref. 15, they are defined at the bottom of the n -th layer.)

Introducing W_n^{pq} matrices following Ref. 15, which are defined by

$$\begin{pmatrix} T_n \\ R_0 \end{pmatrix} = \begin{pmatrix} W_n^{tt} & W_n^{tr} \\ W_n^{rt} & W_n^{rr} \end{pmatrix} \begin{pmatrix} T_0 \\ R_n \end{pmatrix}, \quad (\text{E3})$$

and using the recursion formulae involving M_{n+1}^{pq} matrices at the n -th interface, i.e.,

$$\begin{pmatrix} T_{n+1} \\ R_n \end{pmatrix} = \begin{pmatrix} M_{n+1}^{tt} & M_{n+1}^{tr} \\ M_{n+1}^{rt} & M_{n+1}^{rr} \end{pmatrix} \begin{pmatrix} T_n \\ R_{n+1} \end{pmatrix}, \quad (\text{E4})$$

yields the following recursion formulae for W_n^{pq} matrices:

$$\begin{aligned} W_{n+1}^{tt} &= A_n W_n^{tt}, \\ W_{n+1}^{tr} &= M_{n+1}^{tr} + A_n W_n^{tr} M_{n+1}^{rr}, \\ W_{n+1}^{rt} &= W_n^{rt} + B_n M_{n+1}^{rt} W_n^{tt}, \\ W_{n+1}^{rr} &= B_n M_{n+1}^{rr}, \end{aligned} \quad (\text{E5})$$

where A_n and B_n are defined by

$$\begin{aligned} A_n &= M_{n+1}^{tt} \left(1 - W_n^{rt} M_{n+1}^{rt}\right)^{-1}, \\ B_n &= W_n^{rr} \left(1 - M_{n+1}^{rt} W_n^{tr}\right)^{-1}. \end{aligned} \quad (\text{E6})$$

Here W_N^{rt} determines the reflectivity of the whole multilayer, $R_0 = W_N^{rt} T_0$ ($R_N = 0$), from Eq. (E3).

Finally, the field amplitudes T_n, R_n inside the layers can be obtained from Eqs. (E3)-(E6) by

$$\begin{aligned} R_n &= \left(1 - M_{n+1}^{rt} W_n^{tr}\right)^{-1} \left(M_{n+1}^{rr} R_{n+1} + M_{n+1}^{rt} W_n^{tt} T_0\right), \\ T_n &= W_n^{tt} T_0 + W_n^{tr} R_n, \end{aligned} \quad (\text{E7})$$

which must be progressively applied to all the layers starting at the multilayer substrate where $R_N = 0$.

-
- * Electronic address: `drlee@aps.anl.gov`
- † Also at Department of Materials Science and Engineering, Northwestern University, Evanston, IL 60208
- ¹ D. Gibbs, D. R. Harshman, E. D. Isaacs, D. B. McWhan, D. Mills, and C. Vettier, *Phys. Rev. Lett.* **61**, 1241 (1988).
- ² C.-C. Kao, C. T. Chen, E. D. Johnson, J. B. Hastings, H. J. Lin, G. H. Ho, G. Meigs, J.-M. Brot, S. L. Hulbert, Y. U. Idzerda, and C. Vettier, *Phys. Rev.* **B50**, 9599 (1994).
- ³ E. D. Isaacs, D. B. McWhan, C. Peters, G. E. Ice, D. P. Siddons, J. B. Hastings, C. Vettier, and O. Vogt, *Phys. Rev. Lett.* **62**, 1671 (1989).
- ⁴ D. B. McWhan, C. Vettier, E. D. Isaacs, G. E. Ice, D. P. Siddons, J. B. Hastings, C. Peters, and O. Vogt, *Phys. Rev.* **B42**, 6007 (1990).
- ⁵ K. Namikawa, M. Ando, T. Nakajima, and H. Kawata, *J. Phys. Soc. Jpn.* **54**, 4099 (1985).
- ⁶ J. P. Hannon, G. T. Trammell, M. Blume, and D. Gibbs, *Phys. Rev. Lett.* **61**, 1245 (1988); **62**, 2644(E) (1989).
- ⁷ M. Blume and D. Gibbs, *Phys. Rev.* **B37**, 1779 (1988).
- ⁸ M. D. Hamrick, Ph.D. thesis, Rice University, 1994.
- ⁹ J. P. Hill and D. F. McMorrow, *Acta Crystallogr., Sect. A: Found. Crystallogr.* **52**, 236 (1996).
- ¹⁰ S. W. Lovesey and S. P. Collins, *X-ray Scattering and Absorption by Magnetic Materials* (Oxford University Press Inc., New York, 1996).
- ¹¹ J. M. Tonnerre, L. Sève, D. Raoux, G. Soullié, B. Rodmacq, and P. Wolfers, *Phys. Rev. Lett.* **75**, 740 (1995).
- ¹² M. Sacchi, C. F. Hague, L. Pasquali, A. Mirone, J.-M. Mariot, P. Isberg, E. M. Gullikson, and J. H. Underwood, *Phys. Rev. Lett.* **81**, 1521 (1998).
- ¹³ N. Ishimatsu, H. Hashizume, S. Hamada, N. Hosoito, C. S. Nelson, C. T. Venkataraman, G. Srajer, and J. C. Lang, *Phys. Rev.* **B60**, 9596 (1999).
- ¹⁴ D. Haskel, G. Srajer, J. C. Lang, J. Pollmann, C. S. Nelson, J. S. Jiang, and S. D. Bader, *Phys. Rev. Lett.* **87**, 207201 (2001).
- ¹⁵ S. A. Stepanov and S. K. Sinha, *Phys. Rev.* **B61**, 15302 (2000).
- ¹⁶ R. Röhlsberger, *Hyperfine Interact* **123/124**, 301 (1999).

- ¹⁷ S. K. Sinha, E. B. Sirota, S. Garoff, and H. B. Stanley, *Phys. Rev.* **B38**, 2297 (1988).
- ¹⁸ V. Holý and T. Baumbach, *Phys. Rev.* **B49**, 10668 (1994).
- ¹⁹ R. M. Osgood III, S. K. Sinha, J. W. Freeland, Y. U. Idzerda, and S. D. Bader, *J. Magn. Magn. Mater.* **198-199**, 698 (1999).
- ²⁰ D. R. Lee, C. S. Nelson, J. C. Lang, C. T. Venkataraman, G. Srajer, R. M. Osgood III, and S. K. Sinha, submitted to *Phys. Rev. B*.
- ²¹ L. Nevot and P. Croce, *Rev. Phys. Appl.* **15**, 761 (1980).
- ²² D. K. G. de Boer, *Phys. Rev.* **B49**, 5817 (1994).
- ²³ B. Vidal and P. Vincent, *Appl. Opt.* **B23**, 1794 (1984).
- ²⁴ D. K. G. de Boer, *Phys. Rev.* **B44**, 498 (1991).
- ²⁵ D. Bahr, W. Press, R. Jevasinski, and S. Mantl, *Phys. Rev.* **B47**, 4385 (1993).
- ²⁶ S. A. Stepanov and R. Köhler, *J. Appl. Phys.* **76**, 7809 (1994).
- ²⁷ R. E. Camley, *Phys. Rev.* **B39**, 12316 (1989).
- ²⁸ D. R. Lee, Y. J. Park, S. H. Park, Y. H. Jeong, K. B. Lee, N. Ishimatsu, H. Hashizume, and N. Hosoi, *Physica* **B248**, 146 (1998).
- ²⁹ J. C. Lang and G. Srajer, *Rev. Sci. Instrum.* **66**, 1540 (1995).

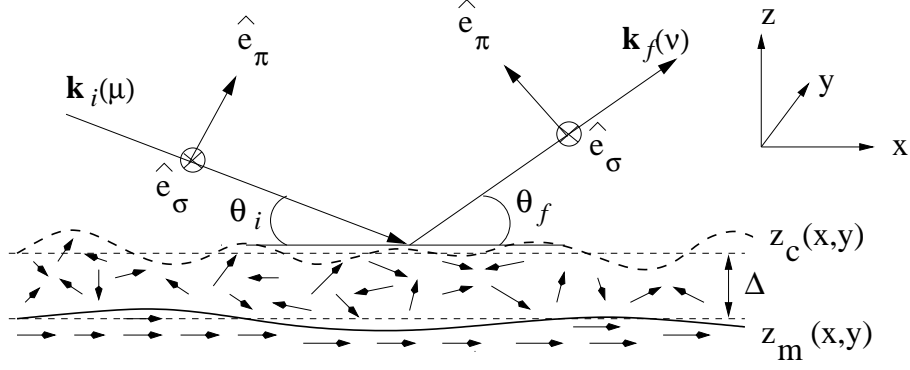


FIG. 1: Schematic of scattering geometry and sketch of the chemical (or structural) ($z_c(x, y)$) and magnetic ($z_m(x, y)$) interfaces, which can be separated from one another by an average amount Δ . Grazing angles of incidence (θ_i) and scattering (θ_f), the wave vectors \mathbf{k}_i and \mathbf{k}_f , and the photon polarization vectors of incidence ($\hat{e}_{\mu=\sigma,\pi}$) and scattering ($\hat{e}_{\nu=\sigma,\pi}$) are illustrated. Small arrows represent the possible orientations of the magnetic moments around magnetic interfaces.

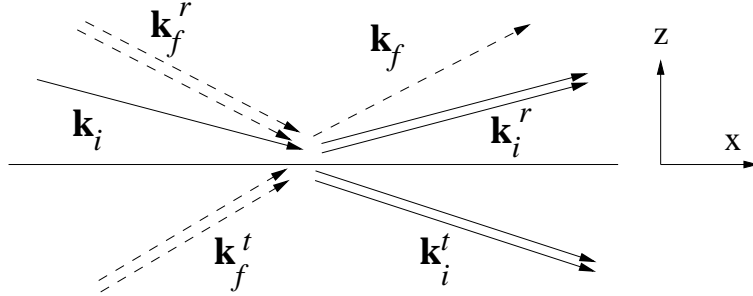


FIG. 2: Schematic of an ideal interface with undisturbed states $\mathbf{E}(\mathbf{k}_i)$ and $\mathbf{E}^T(-\mathbf{k}_f)$. Note two possible waves for each of the reflected and transmitted wave vectors.

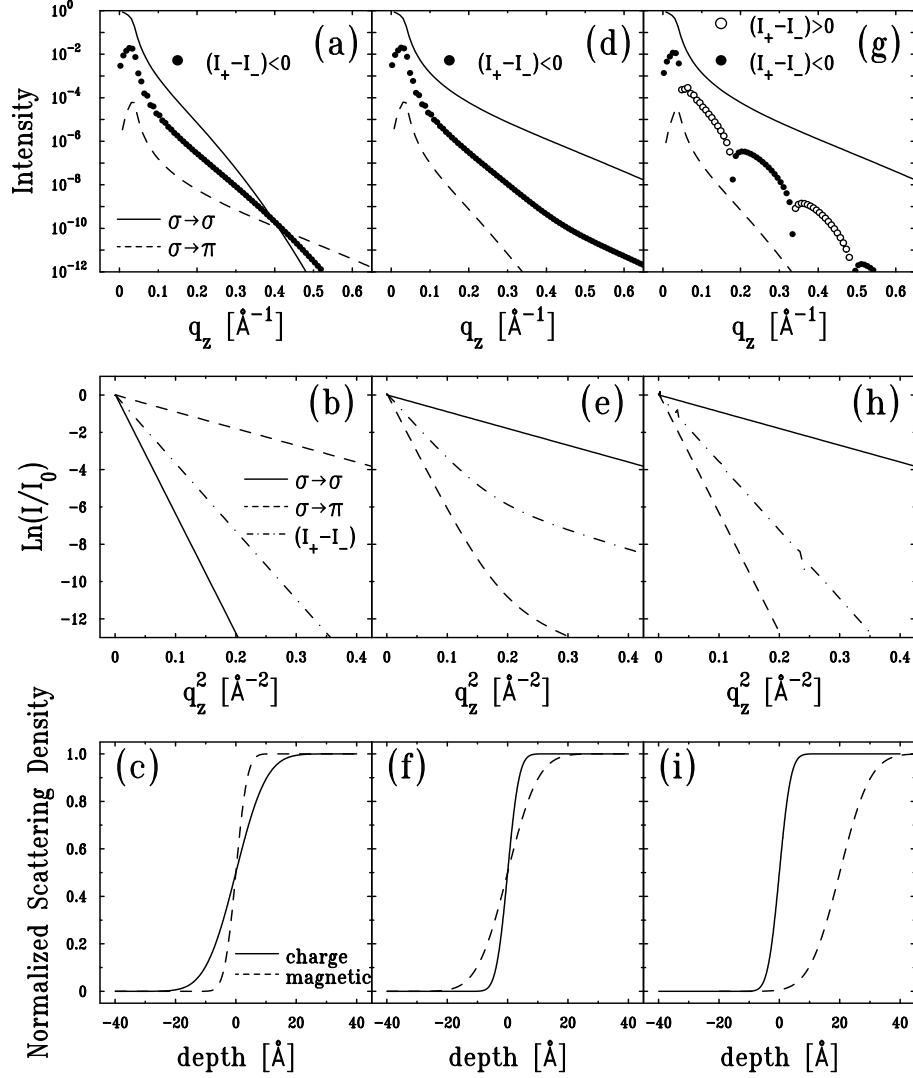


FIG. 3: Calculated x-ray resonant magnetic reflectivities at the Gd L_3 -edge (7243 eV) from Gd surfaces with different interfacial widths for structural (σ_c) and magnetic (σ_m) interfaces: (a)-(c) $\sigma_c = 8\text{\AA}$, $\sigma_m = 3\text{\AA}$. (d)-(f) $\sigma_c = 3\text{\AA}$, $\sigma_m = 8\text{\AA}$. (g)-(i) same as (d)-(f), but with a 20\AA magnetically dead layer. Top panel: reflected intensities of the $\sigma \rightarrow \sigma$ (solid lines) and $\sigma \rightarrow \pi$ (dashed lines) channels, and the differences between the reflected intensities for right- (I_+) and left- (I_-) circularly polarized incident beams (circles). Middle panel: Natural logarithms of the reflectivities with interface roughnesses normalized to those from ideal systems without roughness as a function of the square of the wave-vector transfer. Solid, dashed, and dot-dashed lines represent $\sigma \rightarrow \sigma$ and $\sigma \rightarrow \pi$ scattering, and the differences between I_+ and I_- , respectively. Bottom panel: Normalized scattering density profiles for charge (solid lines) and magnetic (dashed lines) scattering.

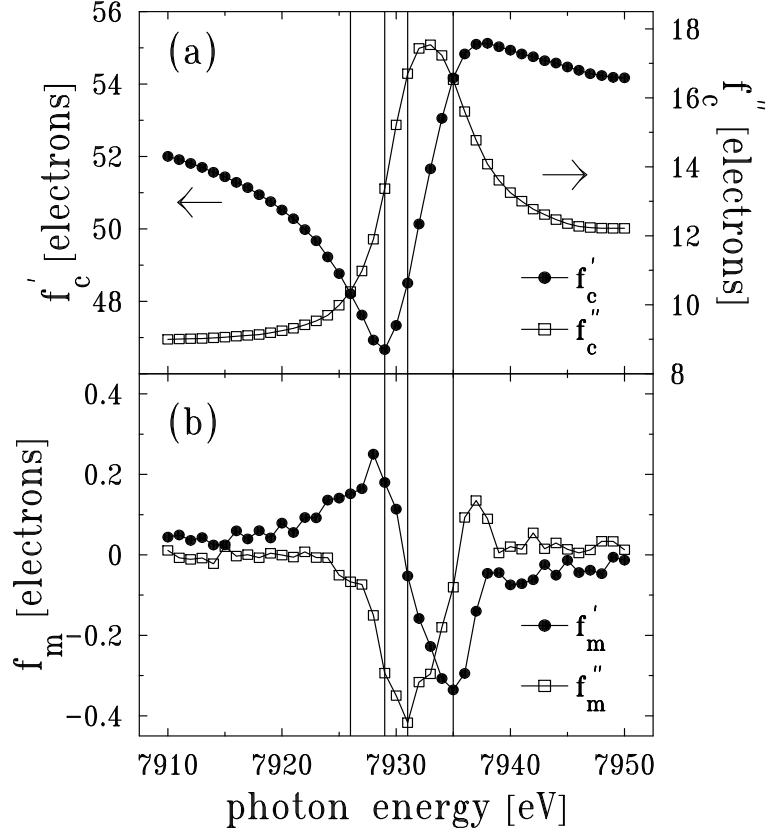


FIG. 4: Charge (a) and magnetic (b) x-ray scattering amplitudes, $f_{c,m}$ around the Gd L_2 -edge obtained from the absorption measurements for a $[\text{Gd}(51 \text{ \AA})/\text{Fe}(34 \text{ \AA})]_{15}$ multilayer. The vertical lines indicate the photon energies, where the x-ray resonant magnetic reflectivities in Fig. 5 were calculated.

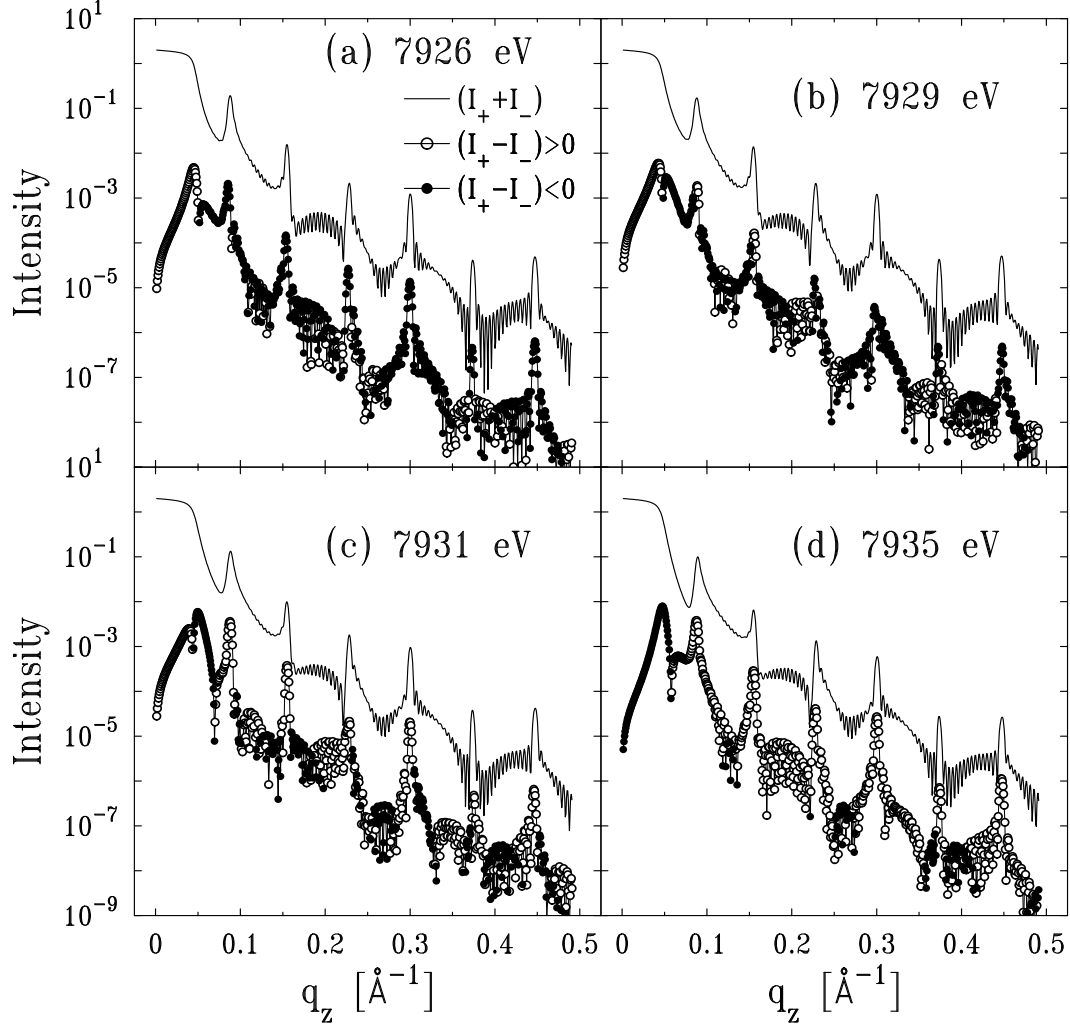


FIG. 5: Calculated x-ray resonant magnetic reflectivities from a $[\text{Gd}(51\text{\AA})/\text{Fe}(34\text{\AA})]_{15}$ multilayer for different incident photon energies indicated in Fig. 4: (a) 7926 eV, (b) 7929 eV, (c) 7931 eV, and (d) 7935 eV. Both structural (charge) and magnetic interface roughnesses are $\sigma_{c,m} = 4.7 \text{ \AA}$ and 3.6 \AA for Fe/Gd and Gd/Fe interfaces, respectively. The solid lines represent $(I_+ + I_-)$ intensities and open (filled) circles represent the positive (negative) values of $(I_+ - I_-)$ intensities.

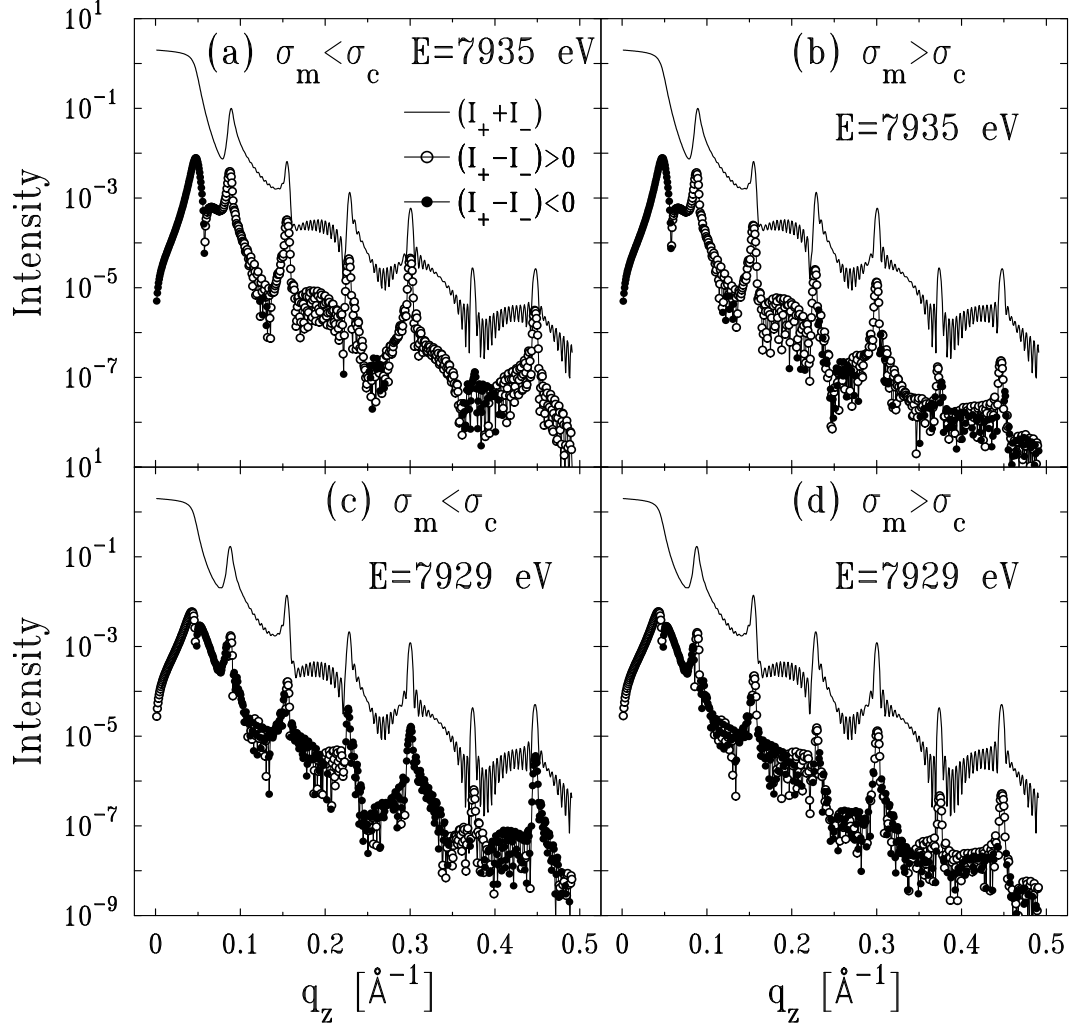


FIG. 6: Calculations with different magnetic interface roughnesses: (a) and (c) $\sigma_m = 2.1 \text{ \AA}$, and (b) and (d) $\sigma_m = 6.2 \text{ \AA}$. All other parameters and symbols are same as those in Fig. 5.

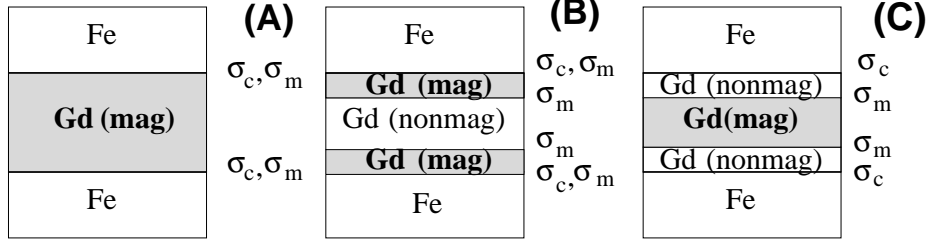


FIG. 7: Models of magnetic structures in Gd layers. Uniform magnetization (A), ferromagnetic moments only near the Gd/Fe interfaces (B), and ferromagnetic moments near the centers of Gd layers between magnetically dead layers (C). While interfaces with “ σ_c, σ_m ” represent both structurally and magnetically mixed interfaces, interfaces with “ σ_c ” (or “ σ_m ”) represent purely structural (or magnetic) interfaces.

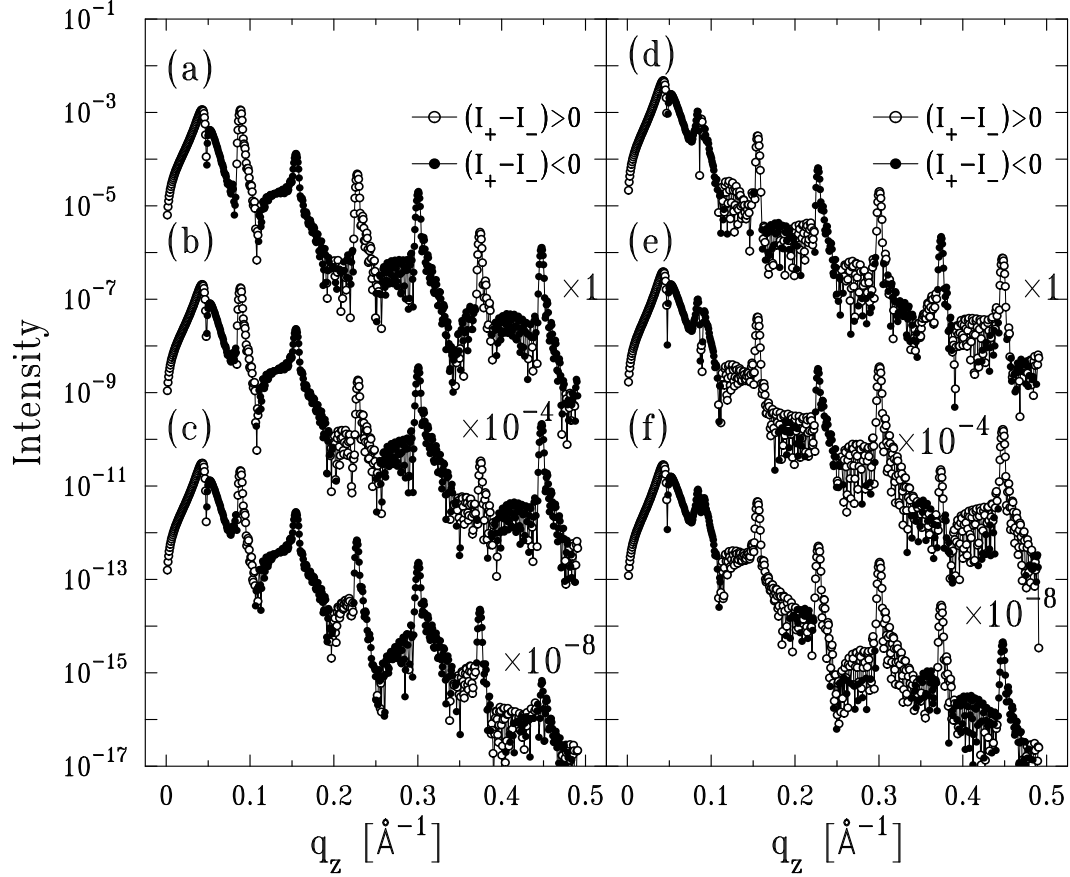


FIG. 8: Calculated $(I_+ - I_-)$ intensities for different magnetization depth profiles in Gd layers. In (a)-(c) ferromagnetic layers exist only near the Gd/Fe interfaces [Fig. 7(B)], and their layer thicknesses are 4.6 Å (a), 8.4 Å (b), and 12.8 Å (c). In (d)-(f) ferromagnetic layers exist in the middle of Gd layers and are sandwiched between magnetically dead layers [Fig. 7(C)], and the layer thicknesses of the dead layers are 4.6 Å (d), 8.4 Å (e), and 12.8 Å (f). All magnetic roughness amplitudes are $\sigma_m = 4.2$ Å, which is effectively same as σ_c , and the photon energy is $E = 7929$ eV. All other parameters and symbols are same as those in Fig. 5.

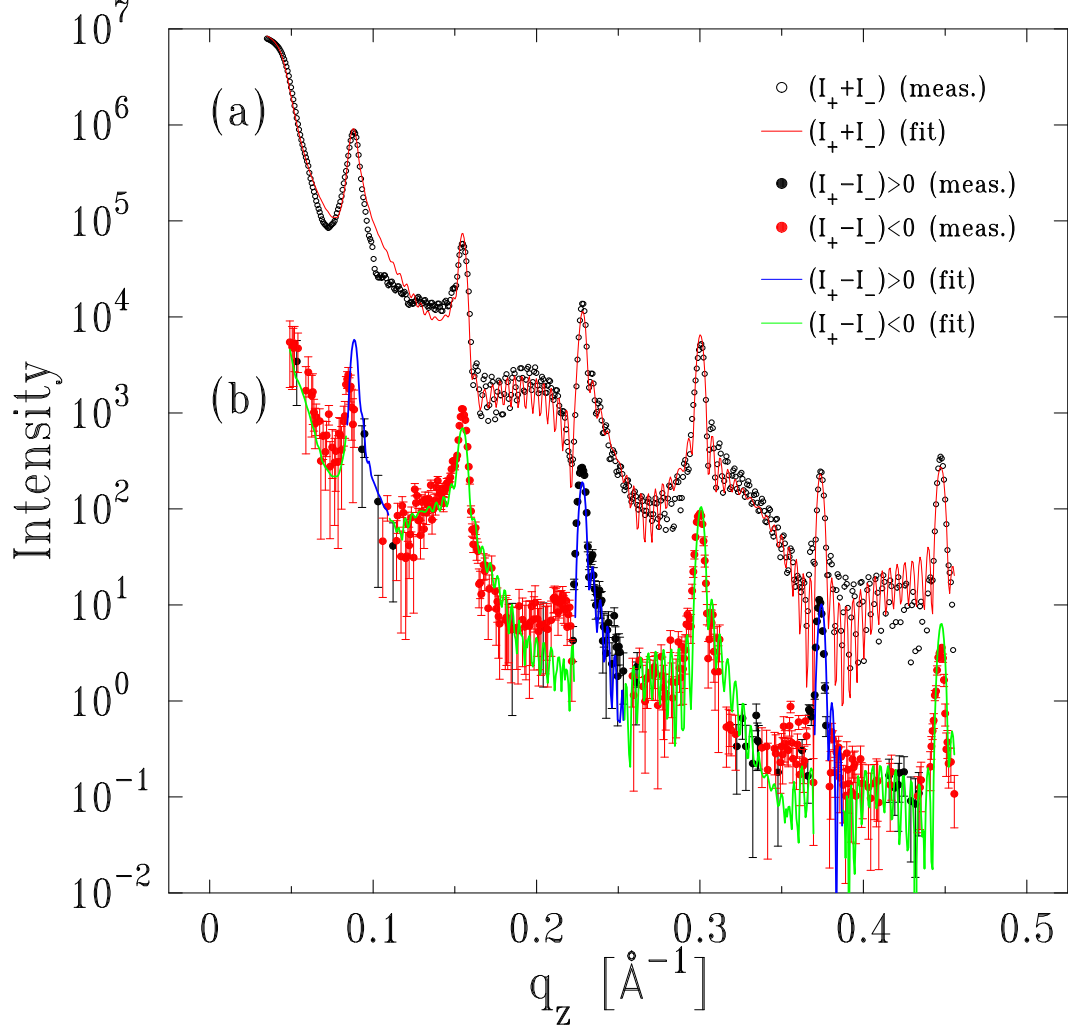


FIG. 9: $(I_+ + I_-)$ [(a)] and $(I_+ - I_-)$ [(b)] intensities measured (symbols) from a $\text{Fe}(34 \text{ \AA})/[\text{Gd}(51 \text{ \AA})/\text{Fe}(34 \text{ \AA})]_{15}$ multilayer near the Gd L_2 -edge (7929 eV). The lines represent the best theoretical fits with the model (B) in Fig. 7. Note that the colors of symbols and lines in $(I_+ - I_-)$ intensities are different for opposite signs of the intensities.

	Incident	
	$\sigma (1)$	$\pi (2)$
reflected (transmitted)	$\begin{pmatrix} M_{11}^{pq} & M_{12}^{pq} \\ M_{21}^{pq} & M_{22}^{pq} \end{pmatrix}$	
$\sigma (1)$		
$\pi (2)$		

FIG. 10: The representation chosen for the elements of M^{pq} matrices with the polarization bases of the incident and reflected (or transmitted) waves. The polarization basis is given by $(\hat{\mathbf{e}}_\sigma, \hat{\mathbf{e}}_\pi)$, as shown in Fig. 1, for the waves in the nonmagnetic medium and $(\hat{\mathbf{e}}^{(1)}, \hat{\mathbf{e}}^{(2)})$, as defined in Appendix A, for those in the resonant magnetic medium, respectively.